PART 3 EXPERIMENTAL PROGRAMME

This work has studied the characteristics and incendivities of the low energy discharges produced by the pulse and capacitive test apparatus. The relationship between these discharges and those to be found in "real world" hazard situations was to some extent explored. The experimental programme falls conveniently into three major areas: a brief investigation of some low energy electrical discharges from the human body and small capacitances, experiments using the capacitive discharge apparatus and software, and experiments using the pulse discharge apparatus and software.

The investigation of electrical discharges from the human body is to clarify some of the characteristics of these discharges, particularly at low stored energies and voltages below the minimum breakdown of air. This area has not to my knowledge been previously investigated. This omission is probably because most workers are concerned with characterising the maximum destructive power likely to occur in practice, which is thought to occur at maximum stored energies and voltages. The low energy region may, however, be of great interest where the most sensitive substances (or electronic systems) are handled. Discharges from the human body represent an important class of discharge source in manufacturing environments, but discharges from charged bodies or surfaces are also of great importance. A complete investigation of these sources is beyond the scope of this work. A description of some discharges from small capacitances is included. These simulate discharges from small metallic objects, for example the blade of a hand tool.

The test methods were applied to the ignition of a gas mixture and a dust layer, as examples of some sensitive materials which had very different characteristics but which were typical of those of interest in hazard assessment. In the process an investigation was conducted of the extent to which discharge characteristics such as discharge current, energy delivery rate and total discharge energy could be predicted, controlled and measured and which of these factors could be important in the ignition process and in the specification of sensitivity.

Some aspects of these questions, for example the ability of these systems to work in the microjoule energy region, have been researched more fully in this work. Other aspects such as the ignition of sensitive powder layers, are of such complexity as to only allow a cursory study, but identify key areas of interest which could be persued by later studies. The following sections present a description of the results of the

3.1 DISCHARGES FROM SMALL CAPACITANCES

The study of metal–metal discharges from small capacitors was of interest in elucidating the impulse discharge associated with the electrode bodies in an ignition apparatus. The impulse at the wavefront of a human body discharge from a metal electrode (such as a handtool, key or ring) is probably similar. Moreover, discharges from small metal objects may be a source of hazard to a sensitive material. Discharges from capacitances in the range 3–92pF using metal electrodes with spacings of 0.1–0.9mm yielded discharge resistance estimates in the range 4–30Ω. The circuit resistance was only 1Ω. Waveshapes ranged from damped ringing sinusoidal to unipolar impulse. As circuit resistance was much less than the discharge resistance, more than 75% of the stored energy appeared in the discharge. Peak currents in the range 10–100A were observed. Discharge durations were in the range 1–20ns, and oscillation periods in the range 3–15ns. Electrode shape had some effect on the discharge form and breakdown voltage. A discharge from a round screw head was more highly damped than that from the slot edge, but the discharge from a needle point was very highly damped.

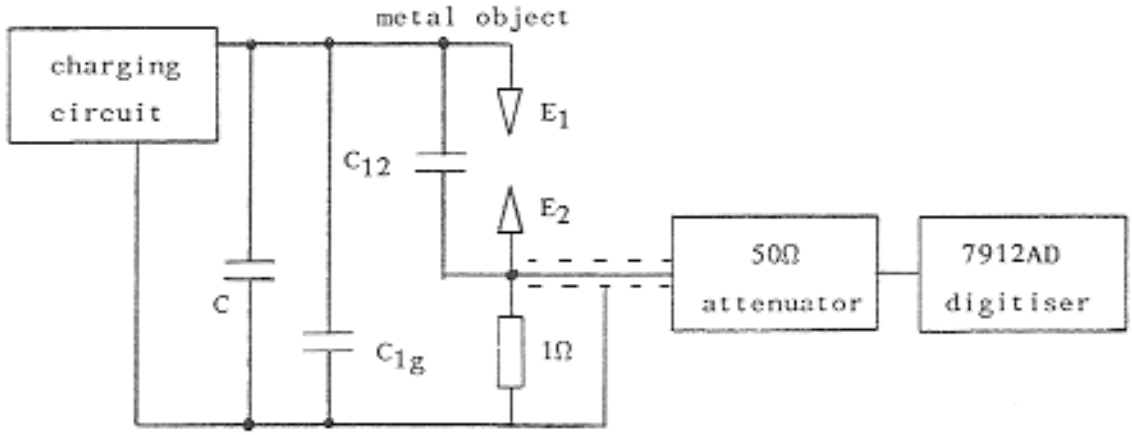

Fig 3.1 Metal object discharge circuit

The discharge circuit was that of fig 3.1. The earthy electrode consisted of a 4.5mm dia by 6mm long brass ferrule with a roughly hemispherical end. This was soldered directly to the central conductor of a 50Ω BNC chassis connector. A solder tag was bolted to each of the four chassis bolt holes of the connector body and a total of ten 10Ω carbon resistors were soldered between these and the central electrode to fabricate a low inductance 1Ω current sense resistor. The high voltage electrode consisted of a round headed bolt screwed into the threaded portion of the 10GΩ charging resistor. A second resistor soldered to a tag connected this to the ESV which allowed measurement of the breakdown potential V_B. The storage capacitor C was soldered directly to a tag on the E1 electrode and to a ground tag on the BNC. The capacitor

or metal object was charged slowly through the charging resistor until breakdown occurred. Single discharges were produced and recorded.

The inductance of the circuit was estimated on the basis of circuit geometry. Grover (1962) gives the inductance of a single turn coil as

$$L = 0.004\ \pi\ a\ [\ln(8a/r)-1.75] \qquad \mu H \qquad (3.1)$$

where r is the wire radius of cross section and a the mean coil radius, in cm. The approximate radius of the discharge circuit was 10mm, and connecting wire radius 0.5mm. This formula yielded an inductance of 16nH for the circuit.

The circuit is an example of the simple C-R-L circuit discussed in section 2.2. The discharge current solutions are of the form

$$I_d = A\ (\exp(\alpha t)-\exp(\beta t)) \qquad (3.2)$$

the two roots α,β of this equation are

$$\alpha,\beta = -(R/2L) \pm \sqrt{(R^2/4L^2 - 1/LC)} \qquad (3.3)$$

The response is oscillatory if

$$\frac{R^2}{4L^2} < \frac{1}{LC} \qquad (3.4)$$

The discharge current is then given by

$$I_d = A\ \exp(-\sigma t)\ \sin(\omega t) \qquad (3.5)$$

where $\sigma = R/2L$ (3.6)

and $\omega^2 = (1/LC - R^2/4L^2)$ (3.7)

$= (1/LC - \sigma^2)$

The exponential term represents the decay of the amplitude of the sinusoid. The decay time constant α could be found by measurement of the amplitude at successive peak times t_1, t_2 where $\sin(\omega t_1) = \sin(\omega t_2) = 1$. The amplitude of the peak current I_{dp2} at time t_2 relative to I_{dp1} at time t_1 is

$$I_{dp2} = I_{dp1}\ \exp(-\sigma(t_2-t_1)) \qquad (3.8)$$

An estimate of the total circuit and discharge resistance R can be made by measurement of this decay time constant. The ratio of the amplitudes of two peaks I_{dp2}/I_{dp1} were measured with the time between peaks (t_2-t_1). From equation 3.8, substituting $\sigma = R/2L$

$$\sigma = \frac{-1}{(t_2-t_1)} \ln \left[\frac{I_{dp2}}{I_{dp1}} \right] \qquad (3.9)$$

$$R = \frac{-2\ L}{(t_2-t_1)} \ln \left[\frac{I_{dp2}}{I_{dp1}} \right] \qquad (3.10)$$

An estimate of the total circuit and discharge inductance L was now required. The oscillation frequency was related to circuit parameters by equation 3.7

$$(2\ \pi\ f)^2 = \omega^2 = (1/LC - \sigma^2) \qquad (3.11)$$

If $1/LC >> R^2/4L^2$ as in a slightly damped ringing waveform then this reduces to the well known relation for a resonant circuit

$$(2\ \pi\ f)^2 = 1/LC \qquad (3.12)$$

which could be rearranged to give

$$L = \frac{1}{(2\ \pi\ f)^2\ C} \qquad (3.13)$$

The frequency $f = 1/(t_2-t_1)$ was measured from the period (t_2-t_1) of the waveform. The effect of non-zero resistance was to reduce the ringing frequency f and reduce the number of cycles seen in the ringing waveform. Hence in practice L was overestimated when significant resistance is present. A better estimate for waveforms approaching the strongly damped condition was obtained by rearranging equation 3.11

$$L = \frac{1}{((2\ \pi\ f)^2 + \sigma^2)\ C} \qquad (3.14)$$

$$= \frac{1}{\left\{\left[\frac{2\ \pi}{(t_2-t_1)}\right]^2 + \left[\frac{-1}{(t_2-t_1)} \ln \left[\frac{I_{dp2}}{I_{dp1}}\right]\right]^2\right\} C} \qquad (3.15)$$

$$L = \frac{(t_2-t_1)^2}{\left\{4\ \pi^2 + \left[\ln \left[\frac{I_{dp2}}{I_{dp1}}\right]\right]^2\right\} C} \qquad (3.16)$$

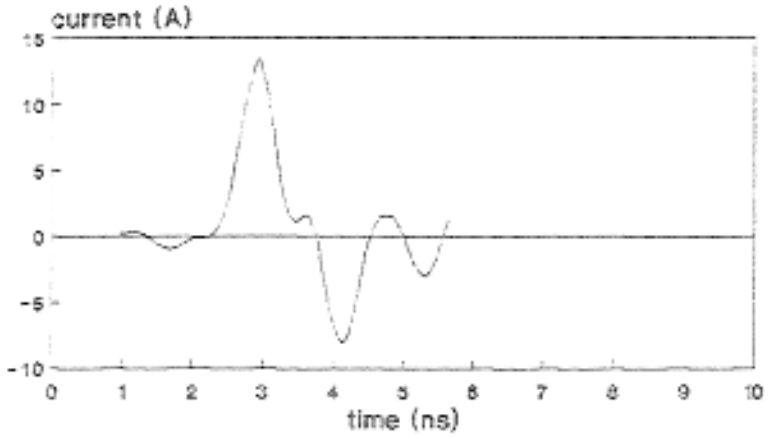

a) d = 0.1mm V_B = not recorded

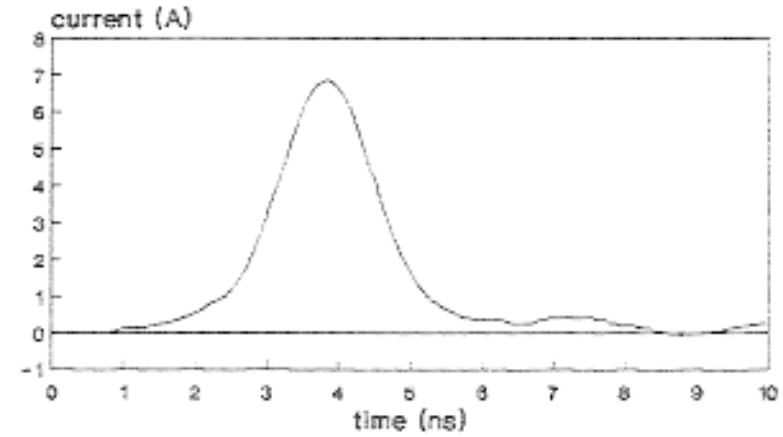

b) d = 0.8mm V_B = 4.1kV

Fig 3.2 Air discharges from a 3pF metal electrode

Discharges were obtained by setting electrode spacings in the range 0–1mm and allowing the capacitance to charge slowly until breakdown occurred. The breakdown voltage was noted from the ESV. Waveforms are shown in figs 3.2 to 3.5. Where oscillatory discharges were observed, the frequencies were measured and the circuit inductance estimated from equation (3.16). Waveforms which had only a positive peak I_{dp+} and a small negative peak I_{dp-} were analysed in the same manner, but equation 3.16 was modified as the frequency f was now given by $f = 1/2(t_2-t_1)$. This led to a modified form of equation 3.16

$$L = \frac{(t_2-t_1)^2}{\left\{ \pi^2 + \left[\ln \left[\frac{I_{dp2}}{I_{dp1}} \right] \right]^2 \right\} C} \qquad (3.17)$$

The discharge data are summarised in tables 3.1–3.3. The mean measured inductance was 38nH (compared to 16nH calculated) but values varied in the region 5–80nH. Discharge inductive effects may account for some of the difference, and experimental error was difficult to quantify. No relation could be discerned between the inductance values and the discharge gap or storage capacitance. A summary of the waveform data and calculated R and L results is given in table 3.1. The first part of the table gives

the data from waveforms having at least two positive peaks and calculated using equations 3.16 and 3.10. The second part of table 3.1 gives data from waveforms having one positive and one negative peak and calculated using equations 3.10 and 3.17. The inductance values were more varied for these waveforms.

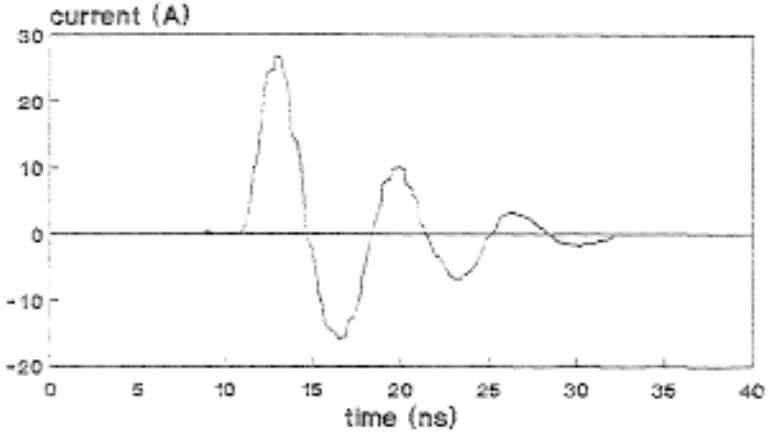

a) d = 0.1mm V_B = 1.1kV

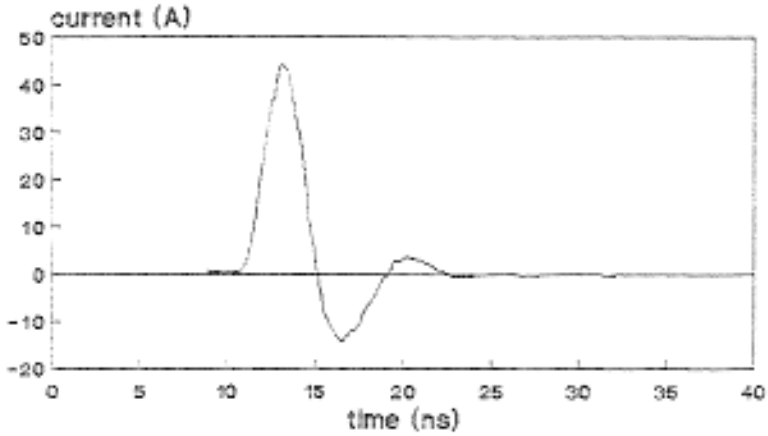

b) d = 0.3mm V_B = 2.1kV

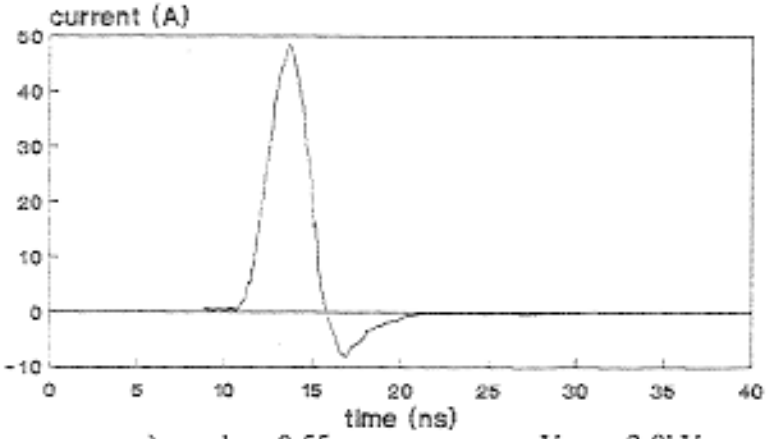

c) d = 0.55mm V_B = 2.8kV

Fig 3.3 Air discharges from a 35pF capacitor and metal electrode

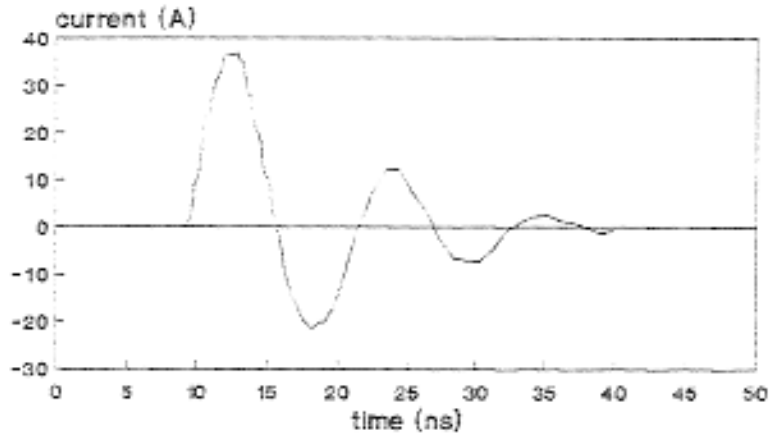

a) d = 0.1mm V_B = 1.0kV

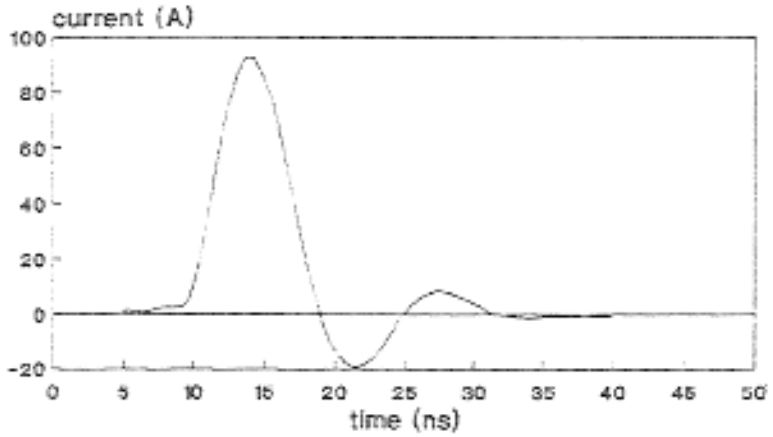

b) d = 0.8mm V_B = 4.0kV

Fig 3.4 Air discharges from a 92pF capacitor and metal electrode

The discharge showed some dependence on electrode form. (fig 3.5) The discharge between rounded electrodes was highly damped at d=0.8mm and but less damped if the discharge occurred from the slot edge in the electrode. A discharge from a sewing needle occurred at much lower voltage and peak current and was nearly unidirectional. Discharges from a square cut or wedge cut 0.8mm dia wire end were also highly damped. It appeared that oscillatory nature (and hence lower discharge resistance) was linked with higher peak currents and the discharge occurring from an edge of intermediate radius edge.

Discharge resistance was variable (fig 3.6) but broadly followed the relation

$$\log(R_d) = 2.35 - 0.61 \log(I_{dp})$$

$$R_d = 223\ I_{dp}^{-0.61} \qquad (3.18)$$

This was consistent with the results from the literature given in section 2.2.

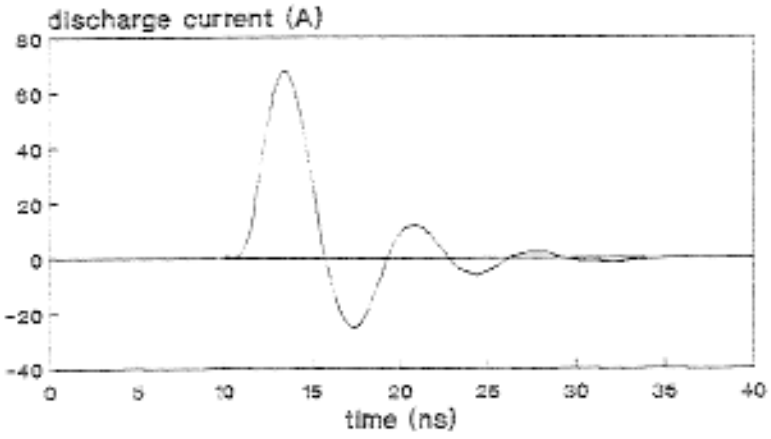

a) Bolt head slot edge d=0.8mm V_B=3.8kV

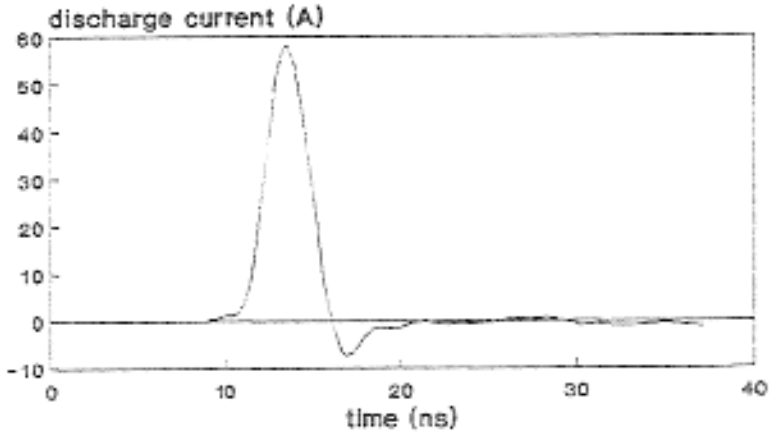

b) Bolt head round portion d=0.8mm V_B=3.8kV

Fig 3.5 The effect of electrode geometry

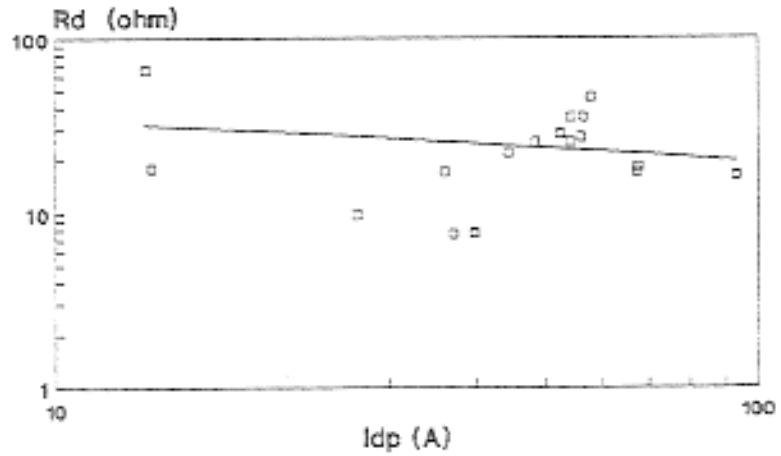

Fig 3.6 Discharge resistance as a function of peak current

Table 3.1 Small capacitance discharge waveform data

Waveform code	V_B (V)	I_p (A)	No of +pks	d (mm)	C (pF)	t_2-t_1 (ns)	L (nH)	R_d (Ω)	electrode form
(calculated using equations 3.16 and 3.10)									
0815AE	1000	37	3	0.1	92	12	38	7.5	bolt head
0815AD	3950	93	2	0.8	92	14	47	16	bolt head
0815AC	1100	39.6	4		92	12	38	7.6	bolt head
0815AG	1100	26.9	3	0.1	35	7	35	9.6	bolt head
0814AG		35.9	2	0.25	35	7.2	35	17	bolt head
0815AH	2100	44.3	2	0.3	35	7	31	22	bolt head
0815AB	4000	56.2	3	0.8	35	8	39	27	bolt head
0816AC	3770	67.5	3	0.8	35	7.5	38	18	bolt slot edge
0814AH		13.4	3	0.1	3	1.8	24	65	bolt head
(one positive and one negative peak, calculated using equations 3.10 and 3.17)									
0814AI		13.7	1	0.3	3	1.4	57	104	bolt head
0815AI	2880	48.4	1	0.55	35	3.2	22	25	bolt head
0814AE		54.3	1	0.65	35	3.9	33	30	bolt head
0814AF		52.5	1	0.9	35	2	6.7	18	bolt head
0815AJ	3500	54.4	1		35	3.3	24	25	bolt head
0816AA	3860	56.5	1	0.8	35	3	18	25	bolt head
0816AB	3800	58.1	1	0.8	35	3.3	21	28	bolt head
0816AD	2200	15.4	1	0.8	35	5.4	72	35	needle
0816AE	3100	32.5	1	0.8	35	5.3	69	35	cut wire
0816AF	2880	24.8	1	0.8	35	5.8	74	45	cut wire
(unidirectional discharges)									
0814AJ		8.2	1		3				bolt head
0814AK		7.8	1	0.9	3				bolt head
0815AA	4100	6.8	1	0.8	3				bolt head

Table 3.2 Summary of peak current and discharge form

(duration/no.of ±peaks/peak current)

Electrode space	C=3pF	C=35pF	C=92pF
0.1mm	0.5/11/13.4	2.2/6/27	4.2/5/37
0.25		2.7/4/35.9	
0.3	1/2/13.7	2.5/3/44.3	
0.55		2.7/2/48.4	
0.7		3.3/2/54.4	
0.8	1.6/1/6.8	3.2/5/56.2	5.7/3/92.9
0.9	1.8/1/7.85	3.3/2/52.5	

Table 3.3 Effect of electrode geometry
(C=35pF, d=0.8mm)

Form	Ip (A)	No of peaks	V_B
Bolt head round part	54.4	2	3500
Bolt head round part	56.5	2	3860
Bolt head slot edge	67.5	5	3770
sewing needle point	15.4	2	2200
square cut 0.8mm wire	32.5	2	3100
wedge cut 0.8mm wire	24.8	2	2880

The discharge resistance was usually an order of magnitude greater than the circuit resistance which consisted mainly of the 1Ω current sense resistance. It follows that the majority of the stored energy was dissipated in the discharge resistance, with a small amount dissipated in circuit resistance. The discharge resistance alone could be sufficient to ensure a unidirectional waveshape. For an unidirectional response, a total resistance of the order of magnitude $R < 70\Omega$ was required. This resistance could be present in these short duration low energy discharges, as a low impedance discharge channel did not have much time to become established and the discharge may not have a high energy density. The circuit equations predicted that an oscillatory response

was more likely if L was increased or C reduced. In practice discharge resistance was likely to increase with a reduction in C, as the energy in the discharge was reduced, and this could counter the effect of the reduction in C. Discharge resistance and inductance were also likely to increase with the discharge length (electrode spacing) for a given discharge current, although as spacing was increased V_B and the peak current were increased. In addition the discharge energy was increased in proportion to V_B^2.

3.1.2 Discharges from test cell electrodes

In ignition experiments a current impulse always occured at breakdown which was explained as the discharge of electrode stray capacitances. Comparison of the impulse with the waveforms recorded from the discharge of small capacitors supports this explanation. The charge transferred in the impulse was relatively constant for a given breakdown voltage, but there could be significant variation in peak amplitude and duration. A high peak was usually of lower duration, and a low peak of longer duration.

Two possible contributors to this impulse were modelled by the stray capacitances C_{12} and C_{1g} (fig 2.9). The pulse due to C_{12} did not pass through the external circuit and was not measured. The pulse due to C_{1g} was measured and was limited in amplitude by the current sense resistance. It was often too short in duration to appear on the full length waveform record, but could be studied by viewing the first few tens of nanoseconds of the discharge. The impulse current could be orders of magnitude greater than the main discharge current. The wavefront of Fig 3.7 showed a 3.3ns pulse of 623mA amplitude, corresponding to the discharge of C_{1g} = 0.6pF with a stored energy of 3.6μJ. The main discharge amplitude was only 4mA. This waveform was recorded with R_s=881kΩ and V_B=3.6kΩ. In most experiments the effect of addition of C_{12} or C_{1g} capacitance in the region 10^{-12}–10^{-11}F was small, except in the first few tens of nanoseconds of the discharge. An increase in either component led to a small decrease in the measured duration, and a small increase in peak current and power of a capacitive discharge. Waveforms obtained using the circuit of fig 2.8 exhibited an extended duration impulse at the wavefront. The decay portion of the second peak was consistent with R_s C values. The duration of the first peak and charge transferred was consistent with the discharge of electrode capacitance through the series resistance R_s.

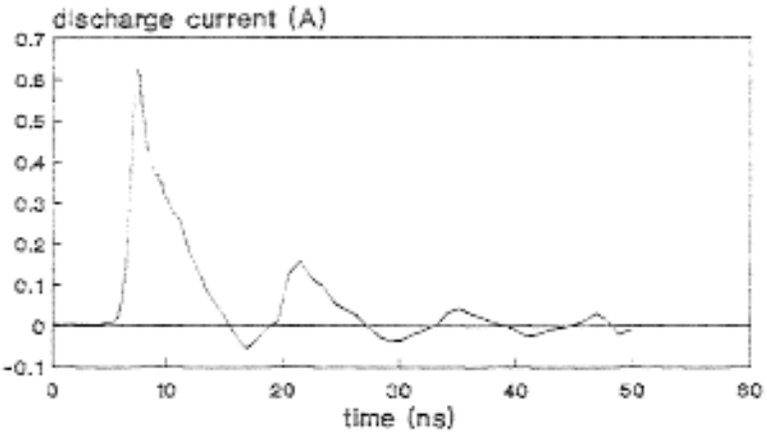

d=0.5mm V_B = 3.6kV R_s = 811kΩ

Fig 3.7 Impulse at the wavefront of a discharge through pyrotechnic

The energy stored in the C_{12} and C_{1g} capacitances were 0.5 C_{12} V_B^2 and 0.5 C_{1g} V_B^2 respectively. The C_{12} stored energy was dissipated only in the discharge, as the charge did not pass through an external circuit (Chubb & Butterworth 1982). A proportion of the C_{1g} stored energy was dissipated in circuit resistance of the measurement circuit. These stray energy components became more significant as the electrode gap was lengthened, due to the V_B^2 dependence. The contribution of C_{12} decreased as gap length increased, because the capacitance decreased with electrode spacing. Thus the energy stored in C_{12} increased as a function of V_B rather than V_B^2.

The magnitude of the stray capacitance C_{1g} could be evaluated by measurement of the charge transferred in the discharge. In practice C_{1g} represented miscellaneous stray components such as the parallel capacitance of the charging resistance as well as the electrode–ground capacitance. Assuming complete transfer of charge,

$$Q_T = C_{1g} V_B \qquad (3.19)$$

The transferred charge could be plotted as a function of V_B. A straight line was formed which had a slope of C_{12}. In practice the assumption of complete charge transfer gave good results. This was probably because the discharge was of very short duration compared to the transit time of electrons across the gap, and the discharge current was almost certainly due to displacement current alone (Barretto et al 1974).

3.1.3 Minimum discharge energy of test cell

The impulse due to electrode capacitance discharge formed the lower limit to the discharge energy which could be achieved. The electrode capacitance was difficult to reduce below 1pF. The minimum breakdown voltage of atmospheric air is approximately 350V at an air gap of around 0.08mm. Hence the lowest practical gaseous discharge energy is of the order 0.06μJ. The presence of other materials in the interelectrode space could alter breakdown characteristics and stored energy, and hence change the minimum energy achieved. A material of $\epsilon_r > 1$ would cause an increase in energy stored in the gap by its effect on the electrode capacitance. A material which reduced or increased V_B would cause a reduction or increase in the stored energy.

3.1.4 Energy contribution of the impulse to the ignition process

Barretto et al (1974,1977) have studied low energy discharges from small capacitances as a source of energy for ignition. They concluded that thermalisation of the discharges was associated with a critical electron density of 10^{17} cm^{-3} (10^{23} m^{-3}). Until thermalisation occurred, the discharge could not act as a significant heat source for ignition, and that MIE corresponded to the onset of thermalisation. From this analysis, it would seem that as long as the charge in the impulse was insufficient to produce the critical electron density, the impulse could not contribute to the ignition process and could therefore be ignored. Barretto et al considered the discharge to be confined to a streamer of radius r_d = 30μm. If the interelectrode gap length was d, the critical electron density ρ_c in the discharge was related to a critical stored charge Q_c

$$Q_c = \rho_c \, e \, \pi \, r_d^2 \, d \qquad (3.20)$$

$$= 4.5 \times 10^{-8} \, d \qquad (C)$$

The electrode gap d is expressed in mm. This analysis applies to short duration discharges where ohmic heating was not important.

3.2 ELECTRICAL DISCHARGES FROM THE HUMAN BODY

A gaseous discharge is possible for body voltages greater than about 350V, but at lower voltages the discharge occurs on or near contact between the electrodes. Little work has been reported with this type of discharge from the human body below the Paschen minimum voltage. In this study positive and negative polarity discharges were observed. The discharges were from the index finger or a small metal object as the body electrode. When a metal electrode was used, the metal could be in contact with the skin or isolated by a dielectric.

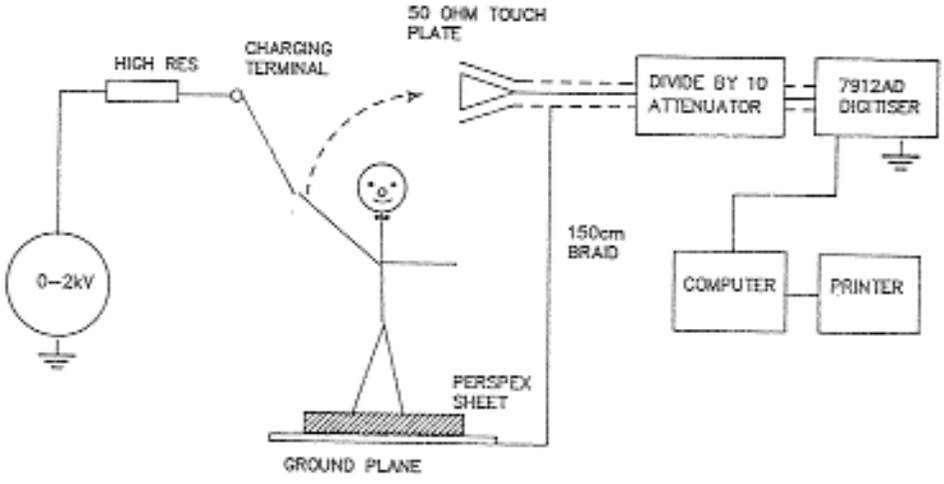

Fig 3.8 Human body discharge measurement system

The test circuit of fig 3.8 was used. The coaxial transmission line probe had a 50Ω characteristic impedance and was described in section 2.1. The subject was separated from the metal ground plane by a perspex sheet. The ground plane was connected to the 50Ω probe outer (ground) conductor by a short length of copper braid to provide a low inductance connection. The subject was charged by touching a charging electrode which was connected to the high voltage power supply via a high (1GΩ) resistance for safety. Power supply voltage less than 1.5kV was measured using a Beckman 4410 DVM. Voltages above 2kV were measured using a Pye electrostatic voltmeter. The body voltage was assumed to be equal to the power supply voltage before discharge. This assumption was justified as the leakage losses to ground were small and corona discharge was negligable at the voltages used. The low leakage was verified using an electrostatic voltmeter during a dummy run of the test sequence. The body lost negligable potential between releasing the charging electrode and discharging to the probe surface. The first 20–50ns of waveform was examined in order to determine its risetime, and whether an impulse was present at the wavefront. The subject in these experiments stood on a 12mm thick dielectric sheet and had a capacitance of 130pF, measured by a capacitance bridge.

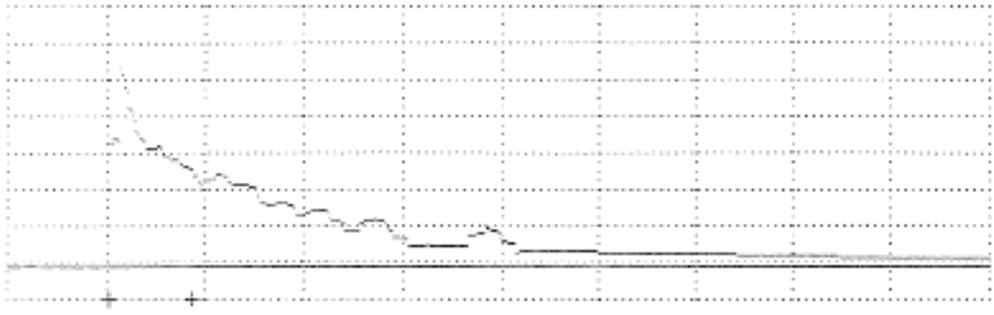

V_B = 1kV vertical 40mA/div horizontal 200ns/div

Fig 3.9 Human body discharge from finger V_B=1kV

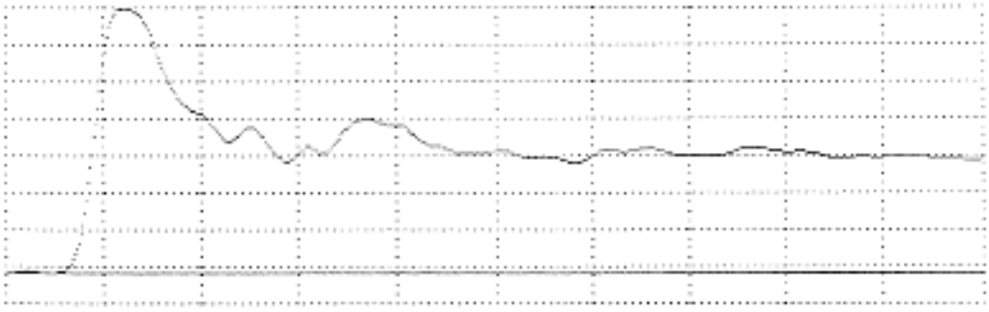

a) Vertical 0.1A/division horizontal 2ns/division

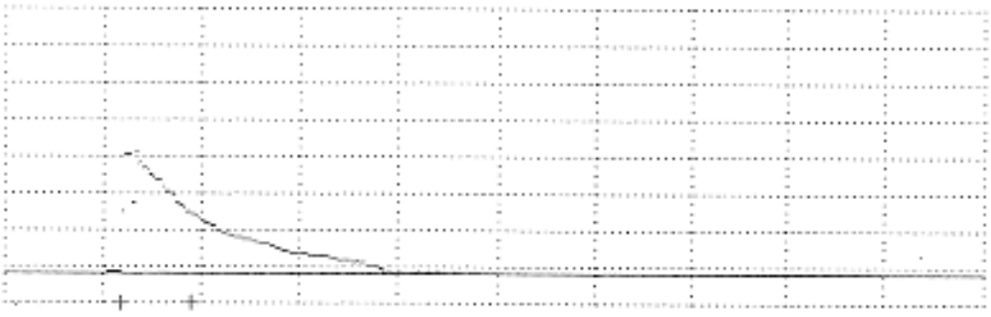

b) Vertical 0.1A/division horizontal 100ns/division

Fig 3.10 Human body +200V discharge from screwdriver

Figure 3.9 shows a discharge from a finger obtained with a body potential of +1000V. Waveforms for −1000V were similar, both waveforms having a fast rise, and decay times of several hundred nanoseconds. Positive and negative waveforms showed risetimes of the order 1ns, probably limited by the measurement equipment. There was little sign of a high amplitude impulse at the wavefront. Peak currents were variable around approximately 200mA for positive and 500mA for negative discharges.

When a metal electrode was used at 1kV, peak currents were greater than the 2A maximum measurable using the test arrangement. The observable portions of the waveforms appeared to be similar to those obtained at lower voltages with metal electrodes. At voltages below the Paschen minimum, discharges from a metal electrode were significantly higher in amplitude than those obtained from a finger, and exhibited a pronounced impulse at the wavefront. With the body charged to ∓200V, a discharge from a screwdriver blade (hand in contact with blade) (fig 3.10a) showed an impulse of 1−2ns in duration, having a peak amplitude of 700mA or greater. The amplitude and duration observed were probably limited by the risetime and bandwidth of the measuring system. After the impulse the waveform settled to 300mA and decayed with a duration of 72ns (fig 3−2.10b). The discharge was similar when a metal object as small as a 9mm length of 0.2mm diameter wire was used as an electrode. The impulse was reduced in amplitude and duration as the electrode size reduced.

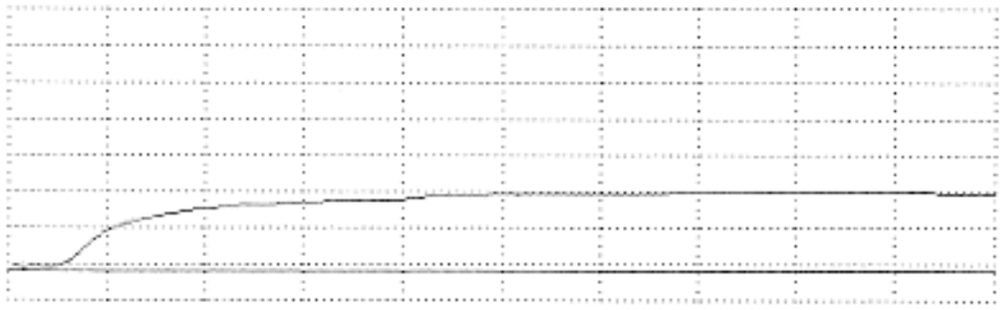

a) Vertical 2mA/division horizontal 2ns/division

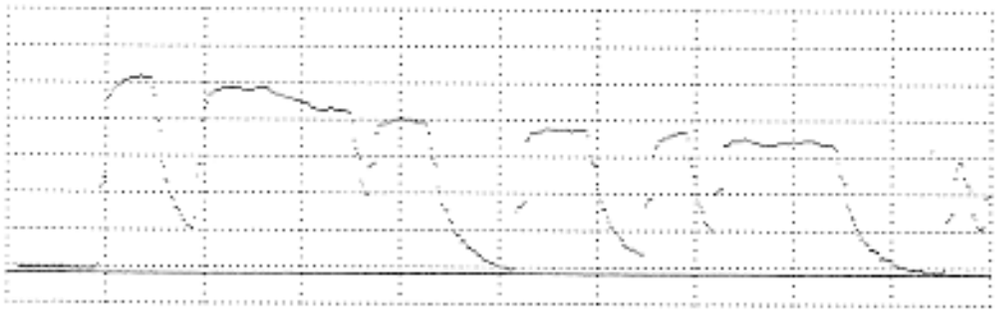

b) Vertical 2mA/division horizontal 100ns/division

Fig 3.11 Human body +200V discharge from finger

A finger discharge from +200V showed a relatively slow rise over several nanoseconds to a peak value of up to 10mA, with no impulse associated with the wavefront (fig 3.11a). On a longer time scale the waveform (fig 3.11b) was often seen to consist of a series of pulsations spread over a duration of several microseconds. The rise of a −200V finger discharge was very slow and of very low amplitude, rising over several

microseconds to a peak of 2mA (fig 3.12). The initial part of the discharge was not detected due to the low amplitude and very slow rate of rise. The waveform exhibited no pulsations and had durations in the region 10–100μs.

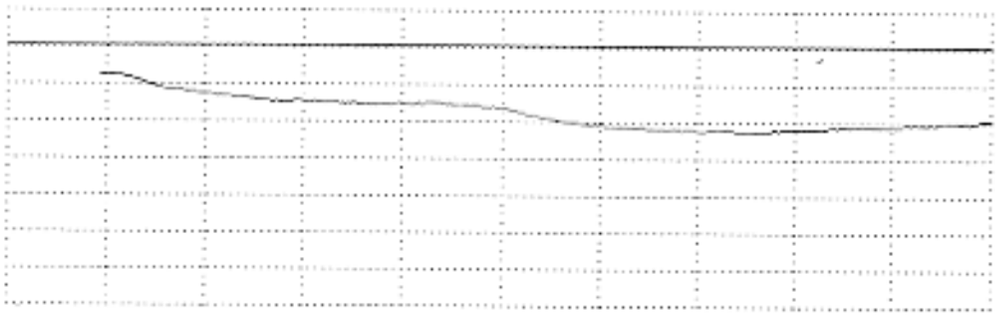

Vertical 1mA/division horizontal 100ns/division

Fig 3.12 Human body –200V discharge from finger

3.2.2 The modelling of human body discharge phenomena

Human body circuit models (fig 1.10) generally represent body charge storage by a capacitance C_b. A resistance R_b models the series resistance of body tissue. Sometimes a series inductance L_b is included. This type of model will here be referred to generically as the C–R–L model. Other componenents may also be included to represent various phenomena. The C–R–L model can be seen to represent some of the waveforms obtained in this study. In particular the waveforms obtained from a body charged to a voltage above the minimum breakdown potential of air, and those obtained using a metal–metal electrode system, generally are of this type.

The effective body capacitance C_b depends on a variety of factors. The area of the sole of the feet, and the thickness of the insulating layer separating the sole from the ground plane, are strong controlling elements. The value of C_b could be simply estimated from the quantity of charge Q_T transferred in the discharge, which is calculated by integration of the current waveform over the duration of the discharge. Assuming complete charge transfer C_b is given by $C_b = Q_T/V_b$, where V_b is the body voltage at breakdown. In a body where one foot is raised from the ground, the decay time constant is significantly shorter than for the same body with both feet in contact, and the value of C_b calculated from the charge transferred is reduced for the same initial voltage. This reduction in capacitance has interesting implications for the body stored energy.

For a body holding a constant charge Q_b, the body voltage is increased from V_0 to V_1 by, for example, raising one foot from the floor, changing the capacitance from Cb_0 to Cb_1.

$$Q_b = C_{b0}\ V_{b0} = C_{b1}\ V_{b1} \tag{3.21}$$

$$V_{b1}/V_{b0} = C_{b0}/C_{b1} \tag{3.22}$$

Stored energy is also raised for $H_s(0)$ to $H_s(1)$.

$$Q_b = 2\ H_s(0)\ /V_{b0} = 2\ H_s(1)\ /V_{b1} \tag{3.23}$$

$$H_s(1) = H_s(0)\ V_{b1}/V_{b0} = H_s(0)\ C_{b0}/C_{b1} \tag{3.24}$$

If the capacitance C_b is halved, the body voltage is doubled, and the stored energy is doubled. In an action like sitting on an insulating stool, both feet may be removed from the floor, and the body capacitance can drop dramatically, with a considerable increase in body voltage and energy. In one experiment two waveforms were taken under similar conditions from a subject. The shorter duration discharge of higher ampiltude occurred when the subject had lifted one foot from the floor subsequent to charging their body. A second, longer duration lower amplitude discharge was recorded when the subject stood with both feet on the floor. A typical subject reduced body capacitance from 170pF while standing on both feet to 60pF when seated with no foot-floor contact.

The effective resistance of the body R_b could be estimated from the decay portion of a discharge. Two points (V_1,t_1) and (V_2,t_2) were chosen on a smooth portion of the decay curve, such that $V_2 = 0.5\ V_1$. The decay time $t_{1,2} = t_2 - t_1$ is measured. The decay portion is assumed to be described by

$$V(t) = V_1 \exp(-t/(R_b+R_d)C_b) \tag{3.25}$$

R_d is the resistive contribution of the discharge. As $V_2 = 0.5\ V_1$, the relation reduced to

$$(R_b+R_d) = 1.44\ t_{1,2}/C_b \tag{3.26}$$

When series resistance is > 200Ω, the proportion of stored energy appearing in a gaseous capacitance discharge discharge is often 10% or less (Rose & Priede 1958, and other authors). This suggests that the discharge resistance R_d is 10% or less of the total, and for many purposes the assumption R_d=0 would be acceptable.

The initial peak due to hand capacitance described by Richman and Tasker (1985) was not pronounced in finger discharges below 2kV. A significant peak was not observed in finger contact discharges. In discharges from metal electrodes an impulse was always present at the wavefront. The amplitude and duration of the impulse appeared to be related to the size of the metal object, and amplitude was linearly related to breakdown voltage V_B. These phenomena can be explained as the discharge of the self capacitance C_e of the metal electrode object into the external circuit, and additional capacitors may be added to the C-R-L model to account for the impulse (fig 3.13). The discharge current is in this case limited only by the impedance of the discharge and external circuit to earth, which may be very low. In our circuit, the dominant factors were the discharge impedance, the 50Ω probe characteristic impedance, and the ground link impedance. The transient, although it may contain relatively little energy, may be of great importance in some circumstances due to its amplitude and speed. Frequency components over 1000MHz may be present. I suggest, for example, that in the electronics industry, this phenomenon may be of importance in the electrostatic voltage transient damage of semiconductor devices, or in causing interference to the operation of local sensitive circuitry.

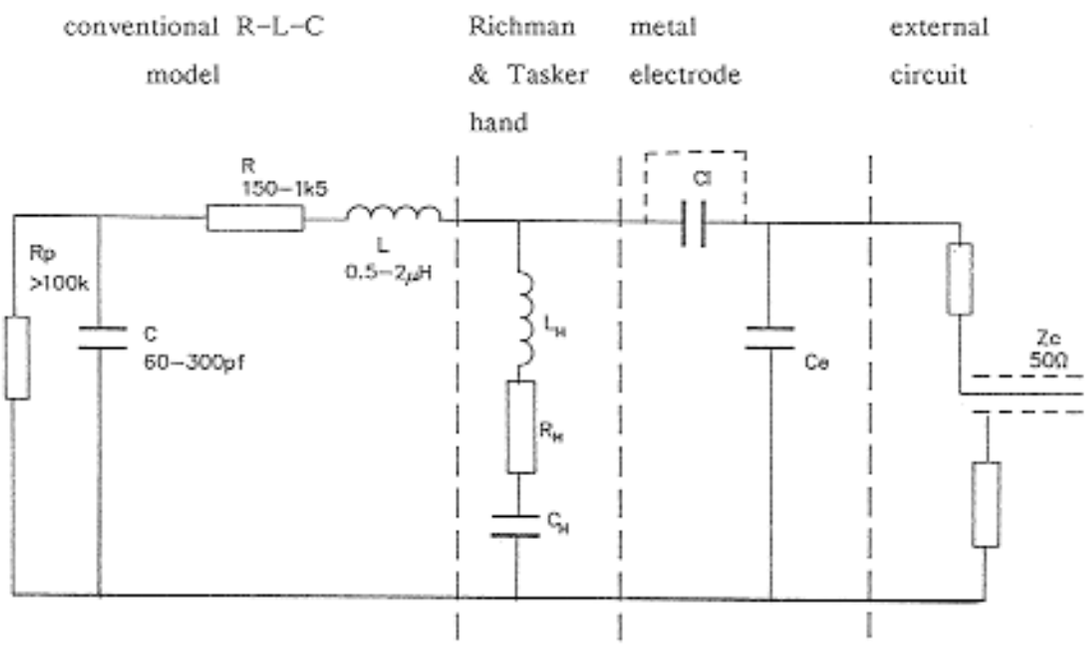

Fig 3.13 Modified human body model

Evidence that the impulse derives from the discharge of the metal electrode capacitance is obtained by consideration of two other results. Firstly, in the case where the electrode was insulated from the hand, eg by the screwdriver handle, only the initial impulse appeared. This condition could be simulated in the body model by the inclusion of a small electrode–ground capacitance due to the metal object. In addition, a series capacitance C_i represented the hand–electrode capacitance, which was short circuited when the screwdriver blade touched the skin. The second confirmation of the origin of the impulse at the wavefront is from observation of the discharges from small capacitances. Reference to the waveforms obtained from the discharge of 3pF (fig 3.2) clearly shows that extremely fast impulses or damped sinusiodal waveforms could be obtained even with circuit resistance as low as 1Ω. Risetimes and durations of <2ns were typical.

It is interesting to compare these waveforms those described in the standard IEC 801–2 (BS6667 Pt 2, 1985) in which is described the generation of test waveforms intended for measurement of electromagnetic compatability in industrial equipment. Some care must be exercised in making this comparison. Firstly, the IEC standard refers to waveforms taken at voltages of 2kV and above, wheras many of my results use voltages an order of magnitude less than this, and quite different discharge characteristics result. Secondly, as the IEC standard points out, the waveforms are dependent on the precise design and construction of the test apparatus. Thirdly, the IEC standard refers to metal–metal discharges only, wheras this investigation has also been concerned with flesh–metal discharges. An interesting and important conclusion from our results is that flesh–metal discharges may have signifcantly different waveforms from those developed by the usual human body model, particularly at voltages less than about 350V. Thus one can only directly compare the 2kV metal–metal discharge results with the IEC standard. There is, however, good agreement between these results and the IEC description. The fast high amplitude peak referred to in IEC 801–2 is clear in the waveforms, and the observed risetime is similar. The exact form and amplitude of the peak is limited by the 0.7ns risetime and 500MHz bandwidth of the Y amplifiers in our equipment – this may also be true when the 1000MHz equipment specified by IEC is used.

The IEC waveform showed a double peak, the second being lower than the first. The first peak may be explained as discharge of the electrode, switch and other stray capacitances, and the second peak as current from the main circuit storage capacitor which is limited in its rate of rise by circuit inductances. If the inductances are sufficiently small, the peak current from the storage capacitance could occur during the initial transient showing only one peak in the waveform. An alternative explanation for the double peak is that an initial impulse may have a positive peak followed by a

negative peak, and this waveform is superimposed on the main discharge of the storage capacitance. Evidence for this mechanism is found in the discharges from small metal objects, which often included a small negative peak following a positive impulse.

The C–R–L model did not effectively represent the waveforms obtained below the minimum breakdown potential of air using a finger–metal electrode system. These finger–metal contact discharges were highly variable in risetime, amplitude and form. Positive finger discharges could show rapid (50–150ns) pulsations whereas negative finger discharges showed slow fluctuations over microseconds. Germer (1958) found that for low voltages an arc is initiated by field emission from the cathode when the gap between approaching electrodes becomes small. Electrode surfaces were activated by the presence of carbon. It is therefore not surprising that a change from a metallic to organic electrode material significantly affected contact discharge characteristics, and that these phenomena depended on polarity.

3.3 CAPACITIVE DISCHARGE MEASUREMENTS

3.3.1 The ignition of 30% hydrogen-air mixture

A brief study of the ignition energy of 30% hydrogen air mixture was designed to show that the discharge measurement system was operational and produced results consistent with those of earlier workers, and to compare them with results of the pulse discharge trials. The 30% mixture was selected as it was close to stoichiometric and gave high sensitivity and low variation of sensitivity to small variations in the mixture. A comparison with Priede's results for the same mixture could be made. The ignition energies of the mixture were determined using the gas test cell described in section 2.4. The results are presented here with discussion of the capacitance discharge phenomena. Part 4 presents further discussion and comparison with other results.

The lowest ignition energy of the 30% hydrogen-air mixture measured using a gap of 0.7mm and 359Ω series resistor was 20μJ. No attempt was made to study the ignition energy as a function of gap length, series resistance, duration or other parameters. The discharge was unidirectional and had a half-amplitude duration of circa 8ns. A typical waveform near the ignition threshold showed a rapid rise in 2-3ns with a distinct peak at the wavefront (fig 3.14) Peak current was typically 7A with a transferred charge of 78nC. The decay portion was somewhat irregular rather than pure exponential.

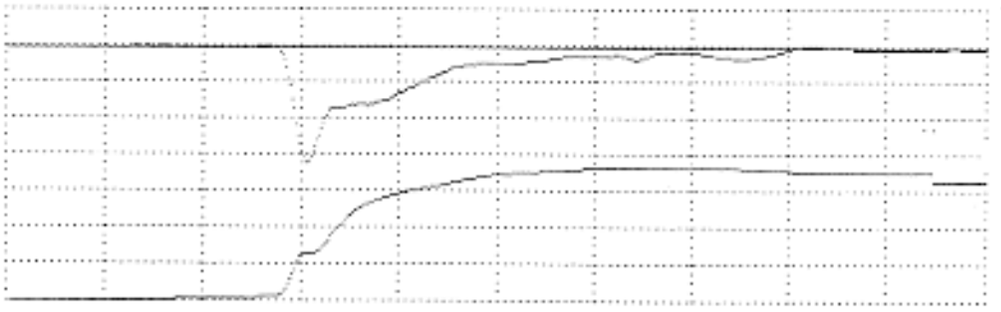

Vertical 2A/div Horizontal 10ns/div

Stored energy 98μJ Discharge energy 20μJ

R_S=359 C_S= 28pF d=0.7mm

Fig 3.14 Typical hydrogen-air ignition test waveform

3.3.2 Analysis of some pyrotechnic ignition data from the literature

Maki (1977) gave the capacitive discharge ignition sensitivity curves (fig 3.16) in which the stored energy was plotted on a linear scale as a function of series circuit resistance on a logarithmic scale. Several pyrotechnic mixtures were studied using a variety of storage capacitance values. The stored energy H_s was calculated from 0.5 C V_B^2.

Many of the curves exhibited sensitive regions. Maki's data was analysed to investigate the sensitive regions as a function of estimated discharge current. The peak current was estimated as $I_{dp} = V_B/R_s$. Experiments with SR10 pyrotechnic showed this relation was accurate to within about 15% for a capacitive discharge in the unidirectional waveform region. Hence the peak current over the approximate range 10^{-3}–10^{0}A could be estimated from an H – R_s graph using the relation

$$I_{dp} = \frac{(2\ H_s/C)^{0.5}}{R_s} \qquad (3.27)$$

The edge of the high resistance sensitive region in Type 1&2 curves was estimated by eye for each graph and the corresponding peak currents were calculated. In addition, the peak currents corresponding to any minima were also calculated. The durations of the waveforms (which would probably be unidirectional for $10^6 > R_s > 10^3\Omega$) could be compared from calculation of the R_s C product. These approximate results revealed three basic types of sensitivity curve (fig 3.15).

Type 1 A sensitive region appeared at higher circuit resistance values.

Type 2 A sensitive region appeared close to $R_s = 0$ as well as at higher circuit resistance values, with a region of significantly lower sensitivity in between.

Type 3 The material showed nearly constant sensitivity from R_s=0 up to a high circuit resistance value.

Type 1 sensitivity was shown by "porous NC powder", "double base powder" black powder and a tracer composition. Type 2 sensitivity was shown by "porous ground NC powder", "igniter composition", "delay composition" and "simulator conposition. Type 3 sensitivity was shown by "incendiary composition". "Delay composition" showed Type 2 sensitivity with a 1300pF capacitor but Type 3 sensitivity to a 50nF capacitor.

In most cases the high resistance sensitivity region of Types 1&2 responses corresponded to an estimated peak current of around 0.5–50mA. In nearly all cases the lower current boundary of sensitivity corresponded to approximately 0.5–2mA. Peak sensitivities were often in the region 0.5–20mA. Some substances had more than one minimum in this range under some conditions. A few substances (eg black powder) had sensitivities extended to at higher discharge currents when the largest storage capacitor (50nF) was used.

Fig 3.15 Three types of ignition sensitivity curve

Moore, Sumner and Wyatt (1956) gave sensitivity curves for the initiator exposive materials service lead azide, silver azide and lead styphnate. Their curves were given in the form of ignition probabilities as a function of series resistance for a fixed capacitance and voltage. These were reinterpreted in a similar manner to above. Service lead azide showed a peak in sensitivity at R_s= 0 and at resistances between 10^5–$10^7\Omega$, and therefore resembled a Type 2 response. The high resistance sensitivity region corresponded to estimated peak currents in the region 0.6–60mA. Sensitivity curves for V_B = 3.2kV (fixed electrode) and 3.7kV (moving electrode) also showed this high resistance sensitivity region with their peaks occurring at a slightly lower resistance than for V_B= 6kV. In all these curves the maximum sensitivity occurred at an estimated peak current of 10mA. Lead styphnate clearly did not show the sensitivity region at high resistance and may resemble a type 3 sensitivity profile. Silver azide, however, showed distinct peaks in sensitivity between 10^4–$10^6\Omega$ as well as at low resistance, and resembled the Type 2 response. Two curves showed a sensitivity peak at an estimated I_{dp} =16mA. Rising sensitivity was apparent in another curve as current was reduced through 28mA (C=400pF, H_s = 16mJ) could be consistant with a maximum around 16mA.

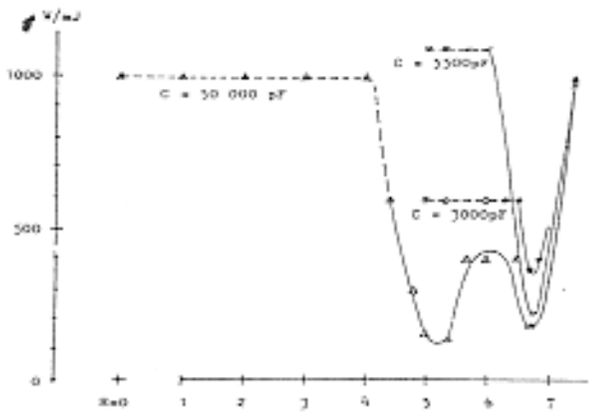

Type 1 – Porous NC powder

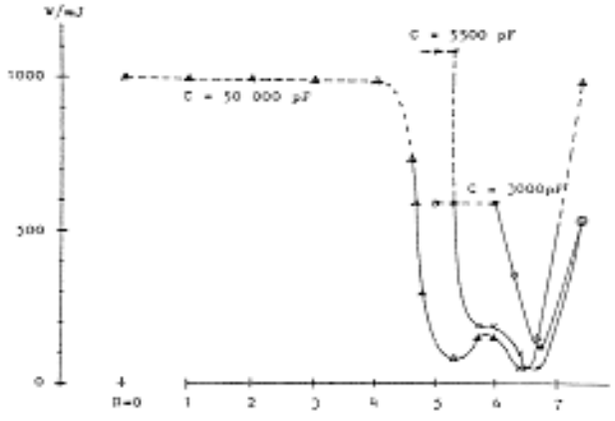

Type 1 – double base powder

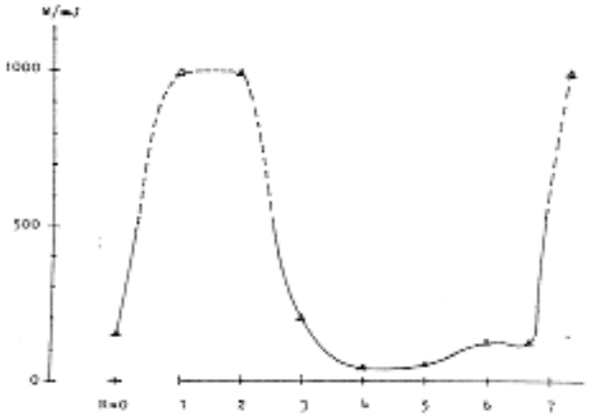

Type 2 – igniter composition

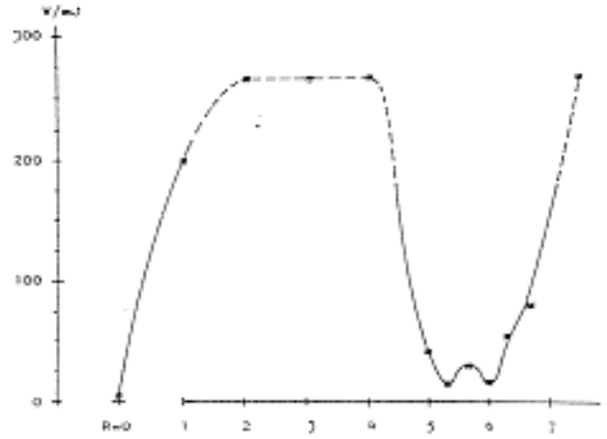

Type 2 – porous ground NC powder

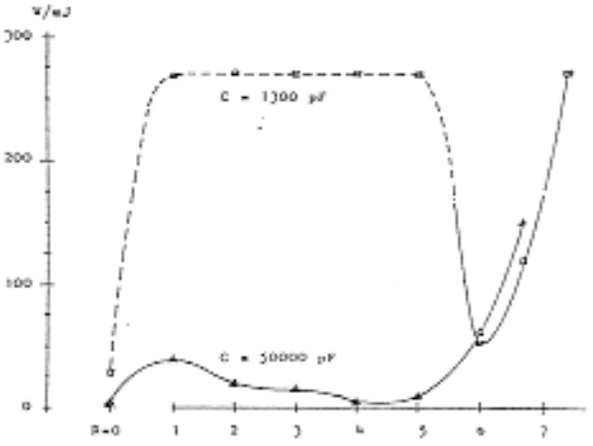

Type 2/3 – delay composition

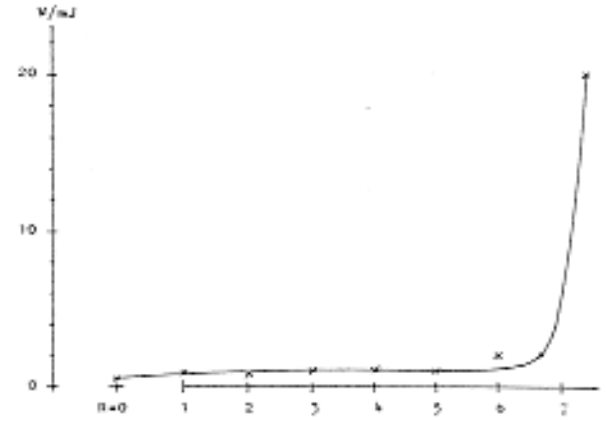

Type 3 – incendiary composition

Vertical – stored energy

Horizontal – log(series resistance)

Fig 3.16 Example pyrotechnic sensitivity curves (Maki 1977)

Kirschenbaum (1973) gave a table showing the minimum ignition energies obtained for lead azide with three values of resistance and four values of capacitance. The values given correspond to peak currents in the region 1–40mA. The lowest values of ignition energies given correspond to estimated peak currents close to the optimum value found from Moore et al's curves.

In summary, of 21 results examined from the literature from various sources all showed reduced sensitivity at $I_{dp} < 10^{3.5}$A. The main incidence of increased sensitivity was in the 10^{-1}–10^{-3}A range. Only 5 results showed sensitivity continuing at $I_{dp} > 10^{0.5}$A. This evidence suggests that the type and characteristics of the discharge through dust in the 10^{-1}–10^{-3}A current range could point to improved incendivity conditions in the ignition of a dust layer. The existance of two sensitivity regions has already been noted by Moore et al (1956), who found regions of sensitiveness to short oscillatory discharges and to long unidirectional discharges, which correspond to the case of low and high circuit resistance respectively. Evidence for this behaviour occurs in a variety of substances. It is possible that different mechanisms are dominant in each sensitivity region. Both regions should be explored in any assessment of the hazard associated with a material.

It is often concluded that the discharge duration is an important factor controlling ignition of dust layers. Of 21 results surveyed most showed sensitivity in the 10^{-2}–10^{-5}s duration range. Only 5 results showed sensitivity at less than 10^{-5}s duration. Six results showed sensitivity at durations greater than 10^{-2}s and only 3 at durations greater than 10^{-1}s. As discharge energy is the integral of discharge power over the discharge duration, it is easily seen that for a given discharge energy, long discharge durations correspond to low discharge powers wheras short discharge durations correspond to high discharge powers. The discovery of an optimum range of discharge durations and powers is not surprising.

3.3.3 The ignition of SR10 pyrotechnic mixture

The ignition of a boron–molybdenum trioxide pyrotechnic was examined using the apparatus of fig 2.21 configured in a capacitance discharge mode using a version of the circuit of fig 2.11a. The pyrotechnic material was a mixture of 25% amorphous boron (0.8–1.4μm diameter) and 75% molybdenum trioxide (2–6μm diameter) particles. The mixture burned with little gas evolution and bright white light output.

Unconfined and part-confined powder arrangements were used in ignition trials. In unconfined trials the electrode was masked by a 0.3mm thick card, and the powder placed in a loose heap on the electrode through a hole in the card. The heap was levelled to the surface of the card, and the card and surplus powder was then lifted off the electrode. This left a thin layer of powder on the electrode. In other trials the powder was partially confined within a 4mm diameter hole in a 1.5mm thick insulating washer. The 1mm diameter stainless steel electrode E1 was lowered into the powder heap before potential was applied to the circuit. The electrode gap was normally set to 0.5mm, and the rod electrode did not usually touch the surface of the unconfined powder layer, but was immersed in the partially confined powder. Some trials used an approaching electrode technique. The minimum electrode gap was set to 0.5mm, ensuring that the discharge occured at an electrode gap of at least this value. Contact discharges were thus ruled out. The electrode was lifted well clear of the powder layer, and the capacitor charged to the required voltage. The electrode was then descended towards the dust layer. This technique allowed accurate determination of the breakdown voltage at the cost of some uncertainty of the discharge gap.

Breakdown voltage, peak current and power at peak current were increased with electrode gap length in the range 0.1mm to 1.0mm, and by the presence of powder in the discharge path. The breakdown voltage with powder was reduced after the first discharge had occurred. This can be explained in terms of an increase in discharge path length when insulating powder was present in the gap, and the suppression of secondary ionisation mechanisms. An initial avalanche and the following discharge must travel a tortuous route between the packed particles, and may interact with the particles. One might anticipate that the more compacted the powder, the more the breakdown voltage may be increased - eventually the "through routes" could be closed by compaction, and the breakdown voltage may approach the value of solid material. The critical compaction may be predictable using percolation theory. After a discharge had occurred, a conduction path was to some degree established. The discharge shock wave could also clear a more direct path through the powder by removing material from the discharge channel, and reaction products could affect breakdown characteritics.

The discharge waveforms observed were categorised into three types - oscillatory, unidirectional and pulse train (fig 3.17). Unidirectional discharges were further subclassified as arc-like, transition or glow like. The type of waveform obtained was largely a function of discharge current, and hence V_B/R_r. These phenomena are explained in the following sections.

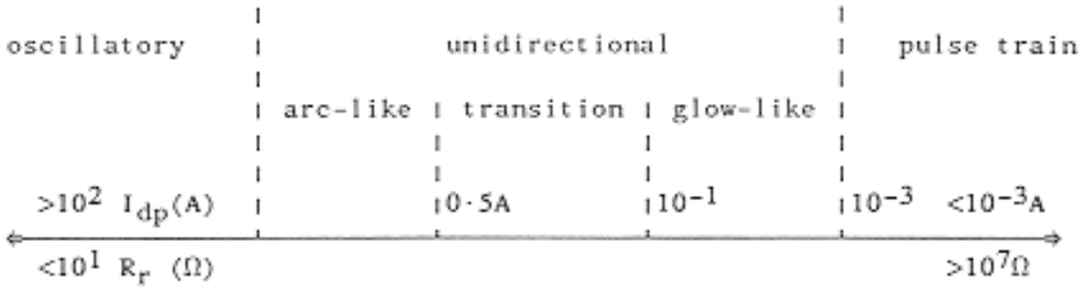

Fig 3.17 Capacitive discharge characteristics as a function of series resistance and discharge current

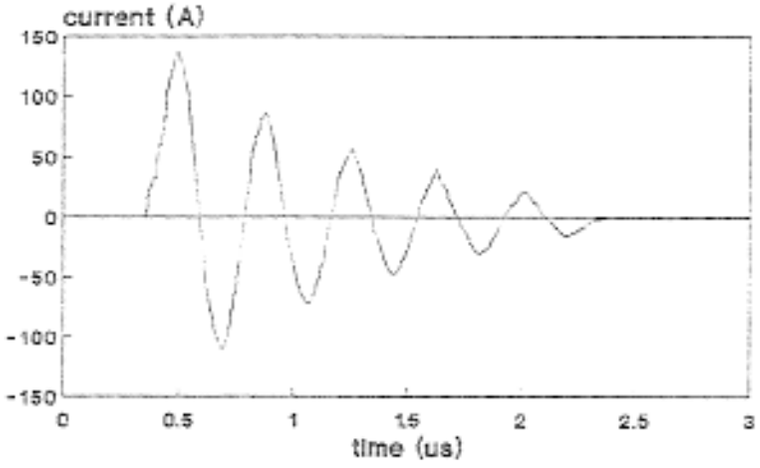

a) Discharge through air

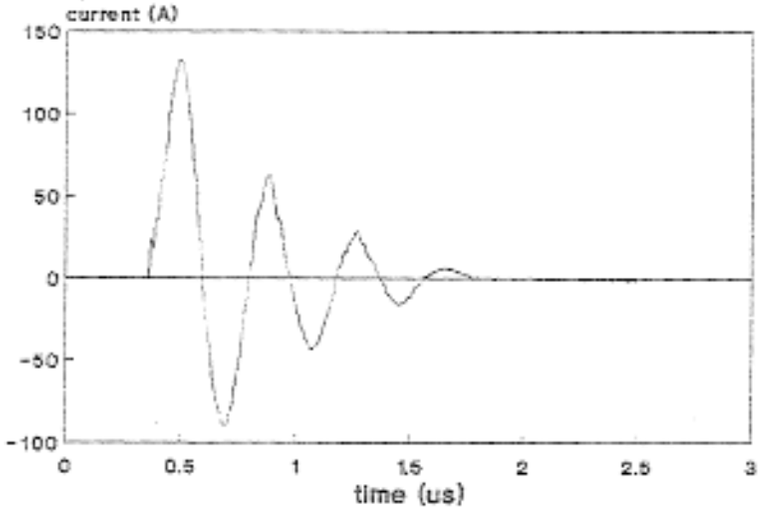

b) Discharge through pyrotechnic

Fig 3.18 Oscillatory discharges

Oscillatory discharges

When low values ($< 10^2\Omega$) of series resistance were used the discharge waveform was a damped oscillatory sinusoid as predicted by the CRL circuit equations given in section 2.2. A discharge through powder typically had lower amplitude and was more highly damped than an air discharge with the same circuit components (fig 3.18). When using low circuit resistance the unconfined powder was difficult to ignite as the sample was blown away from the discharge region. A clear area could often be observed in the dust layer after a discharge, and the dust was visibly dispersed. These effects were reduced and ignition more easily achieved when partial confinement of the powder was used.

Unidirectional discharges

With intermediate ($10^3\Omega < R_r < 10^6\Omega$) circuit resistance values unidirectional waveforms having a fast rising edge and a slower exponential decay were produced, as expected from a damped CRL circuit (fig 3.19, 3.20). Abrupt single or multiple transitions in current were observed in discharges through air and powder at around the 10^{-1}A current level ($R_S \approx 10^4\Omega$). The discharges of fig 3.19 had peak currents in the region 0.4A and entered the arc state soon after breakdown. All exhibited arc-glow transitions during the decay portion, and are typical of waveforms of this peak current value. The discharges of fig 3.20 had peak currents in the region 150mA and entered the arc state for a shorter time if atall. There is little difference between the discharges through air (fig 3.19a, fig 3.20a) and powder (fig 3.20b,c, fig 3.20d) except that a discharge through powder often appeared to terminate at a higher current. The transition current level showed considerable variation associated with a circa 350V change in the discharge voltage. This is consistent with the change between arc and glow discharges described by Gambling and Edels (1954). Reference to an "arc" or "glow" discharge may not be strictly correct in the context of these waveforms as the steady state is not achieved over the short duration, and the presence of powder could modify the discharge processes dramatically. The terms "arc-like" or glow-like", although more cumbersome, will be used here, refering to the low voltage drop (circa 50V) and high voltage drop (circa 400V) discharges respectively. Interestingly, Sumner (1973) noted that a long duration waveform could be exhibit a disruption of the exponential decay, and attributed this to the scattering of ions in the electrode gap at the time of ignition. An examination of his waveforms shows a remarkably constant discharge voltage over a considerable period after "ignition", which may be reinterpreted as the onset of a glow-like discharge.

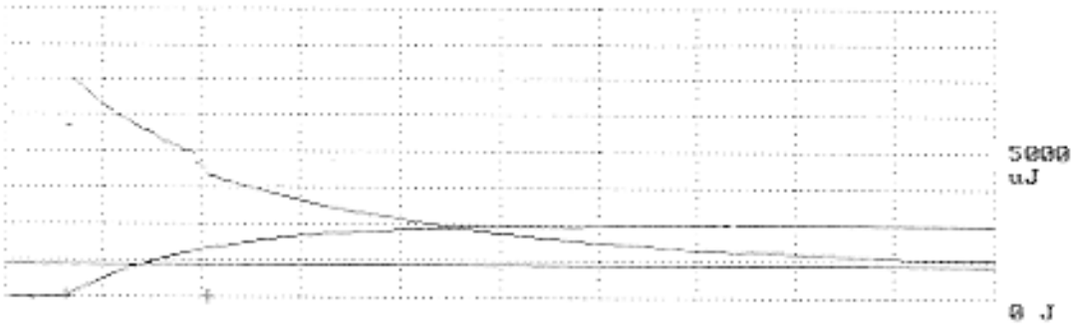

a) Discharge through air

vertical 82mA/div horizontal 5000ns/div

R_S=8kΩ C=1012pF d=0.7mm Discharge energy 2.5mJ

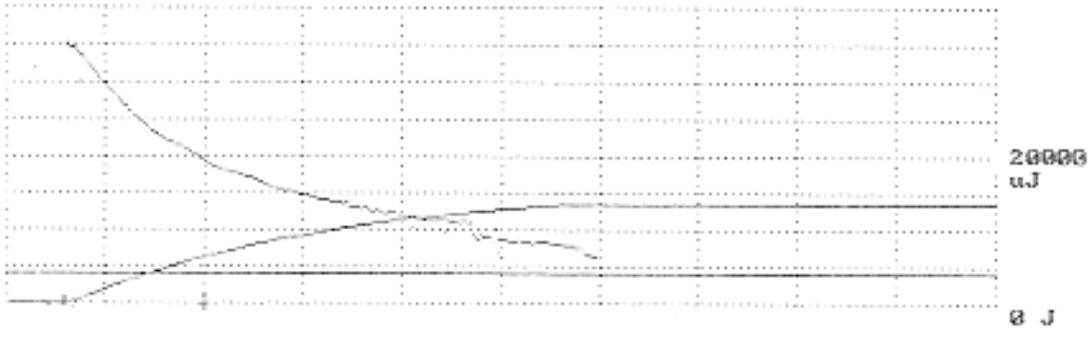

b) Discharge through pyrotechnic (ignition)

vertical 82mA/div horizontal 10μs/div

R_S= 8kΩ C=3097pF d=0.7mm discharge energy 14mJ

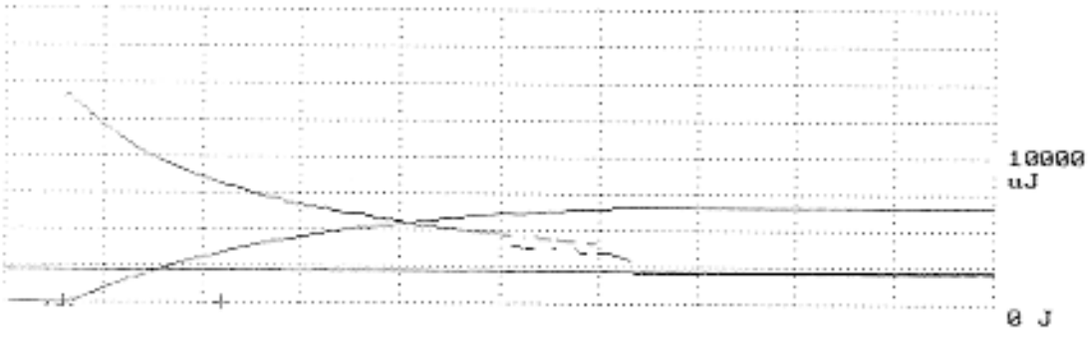

c) Discharge through pyrotechnic (non-ignition)

vertical 82mA/div horizontal 10μs/div

R_S=8kΩ C=3097pF d=0.5mm discharge energy 6.7mJ

Fig 3.19 Unidirectional transition discharges

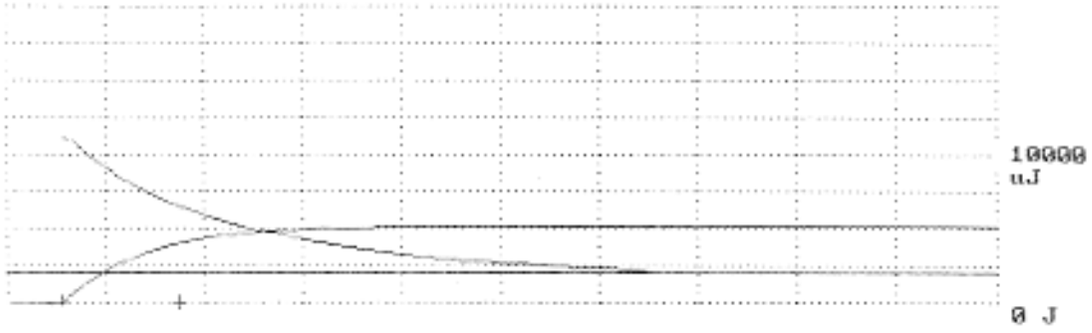

a) Discharge through air

vertical 41mA/div horizontal 20μs/div

R_S=20kΩ C=1012pF d=0.7mm Discharge energy 4.7mJ

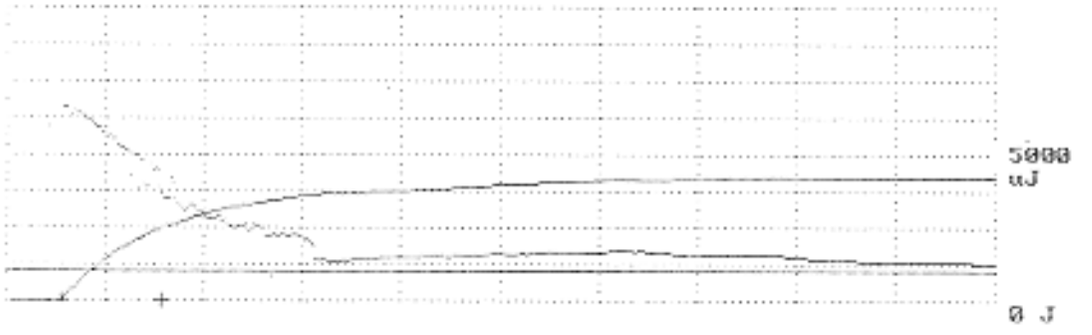

b) Discharge through pyrotechnic (ignition)

vertical 41mA/div horizontal 20μs/div

R_S= 8kΩ C=1012pF d=0.7mm discharge energy 5.2mJ

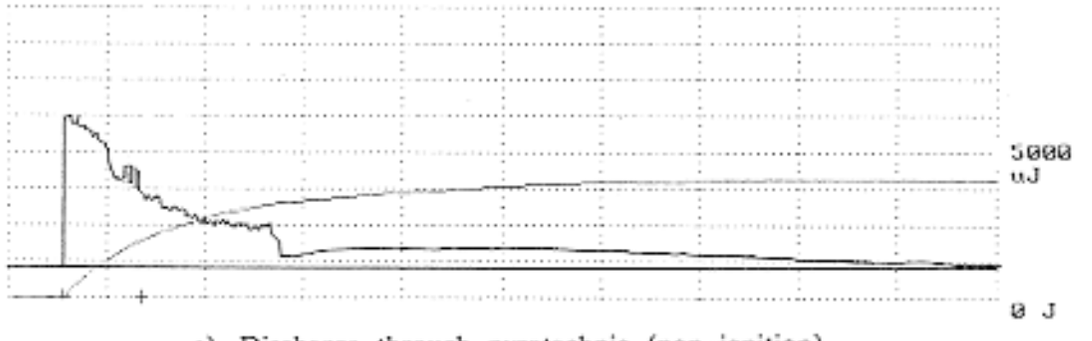

c) Discharge through pyrotechnic (non-ignition)

vertical 41mA/div horizontal 20μs/div

R_S=20.3kΩ C=1012pF d=0.7mm discharge energy 4.1mJ

Fig 3.20 Unidirectional transition discharges

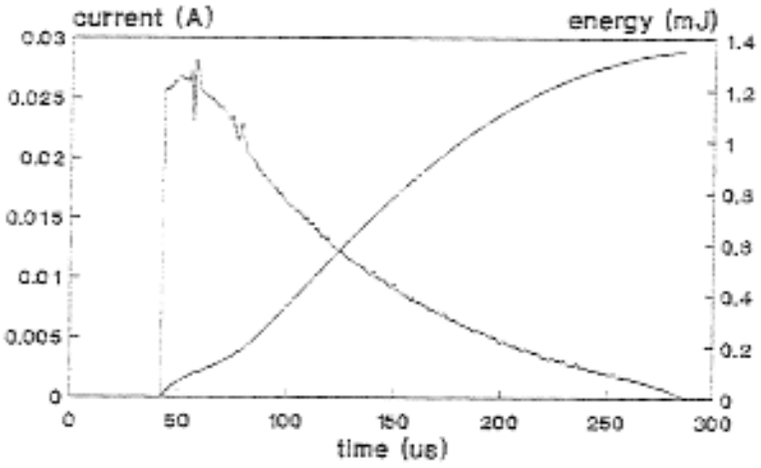

a) Discharge through air

R_s=86.3kΩ C=2030pF d=0.5mm

V_B = 2.6kV Discharge energy H_d = 1.1mJ

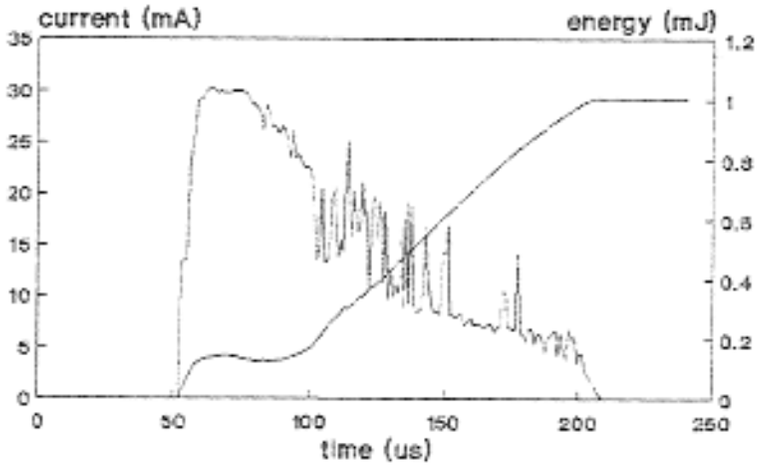

b) Discharge through pyrotechnic

R_s= 88.1kΩ C=2030pF d=0.5mm (approaching)

V_B = 3kV H_d = 1.6mJ

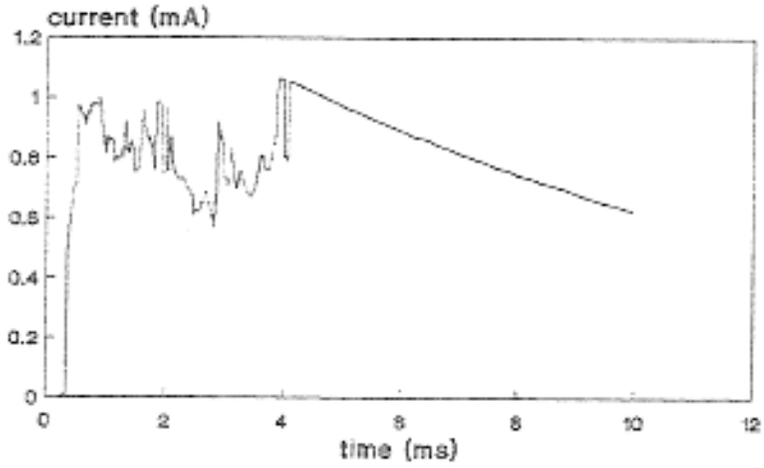

c) Discharge through pyrotechnic

R_s=2770kΩ C=4080pF d=0.5mm (approaching)

V_B = 4kV H_d = not measured

Fig 3.21 Unidirectional glow-like discharges

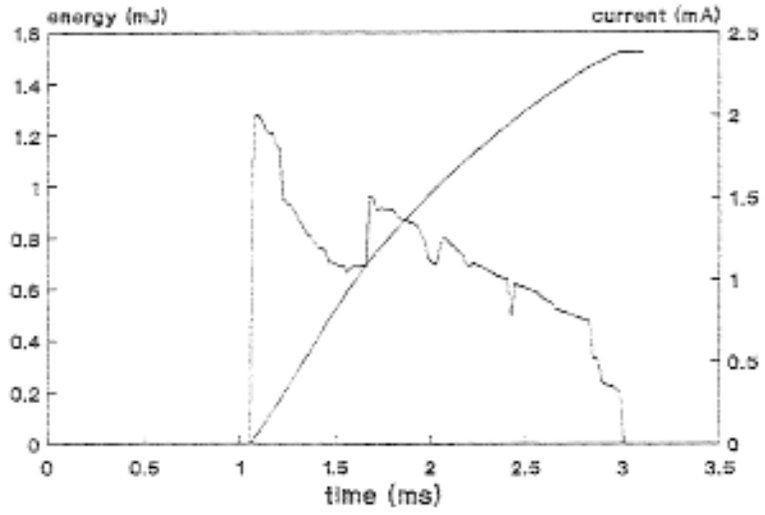

a) Discharge current and energy

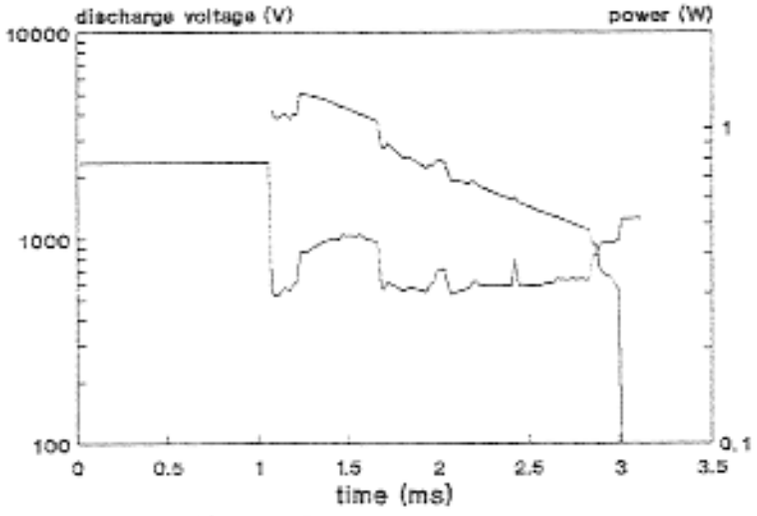

b) Discharge voltage and power

Fig 3.22 Typical unidirectional glow discharge voltage, power and energy characteristics

Lower current discharges often did not exhibit arc-like characteristics atall. The voltage of a glow-like discharge through powder could be extremely variable, featuring rapid fluctuations (fig 3.21). In some conditions a very high discharge voltages were recorded, which may be indicative of an abnormal glow-like discharge state (fig 3.22).

Some discharges featured a disruption of the normal near-exponential decay (fig 3.20a,c and 3.23) in which the current was reduced to a low value but continued to flow for a substantial time. A similar effect was also noted in pulse discharge waveforms described later in this work. This modification of the waveform may be due to the formation of a conductive path through the powder layer by melting of reactants or formation of a conductive reaction product. This hypothesis is further discussed in the context of pulse discharges through pyrotechnic dust.

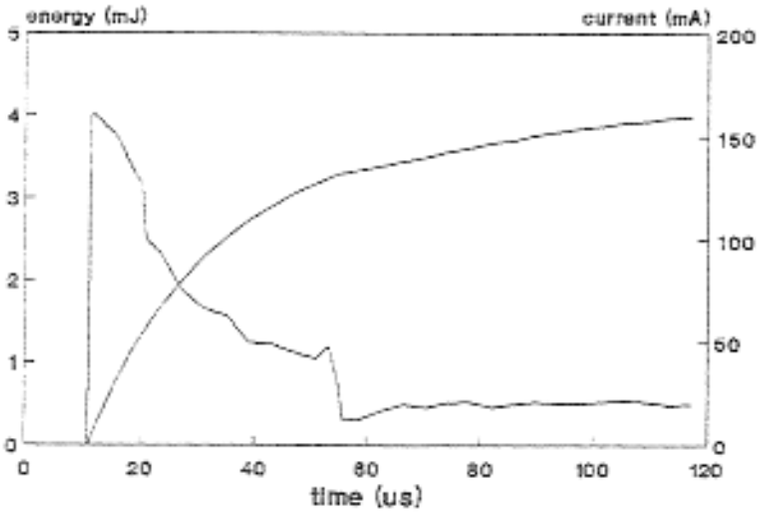

a) Discharge current and energy

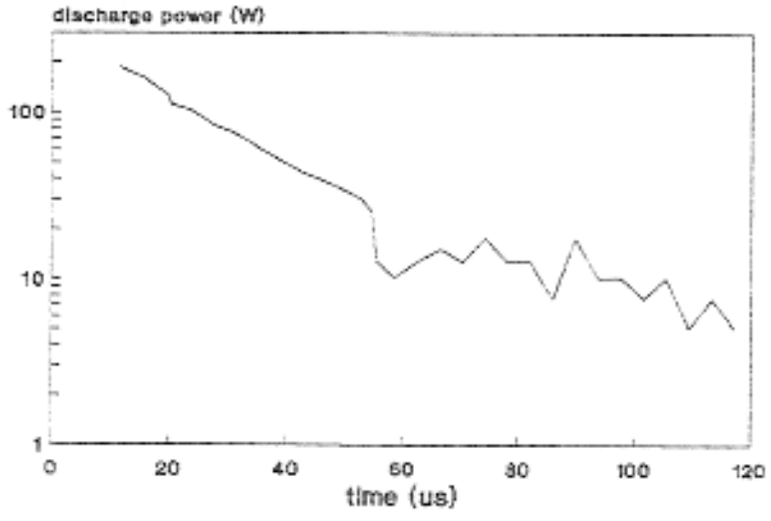

b) Discharge power

Fig 3.23 Unidirectional glow discharge current, power and energy characteristics showing disrupted exponential decay

The power characteristics of some discharges through air and a pyrotechnic powder layer were investigated. Electrode gaps in the range 0–1mm were used. The power current curves for a number of waveforms showed that two discharge states were possible in the 10^{-1}A region. A higher power per unit current was achieved in the state associated with lower currents (fig 3.24). For discharge currents either side of the transition region, the discharge power decayed with the discharge current and the power H_d' approximately followed the relation $H_d' \propto I_d^a$, with values in the range $1 < a < 3.5$ for air. The discharge power can be written in terms of the discharge current and resistance

$$H_d' = I_d^2 R_d \qquad (3.28)$$

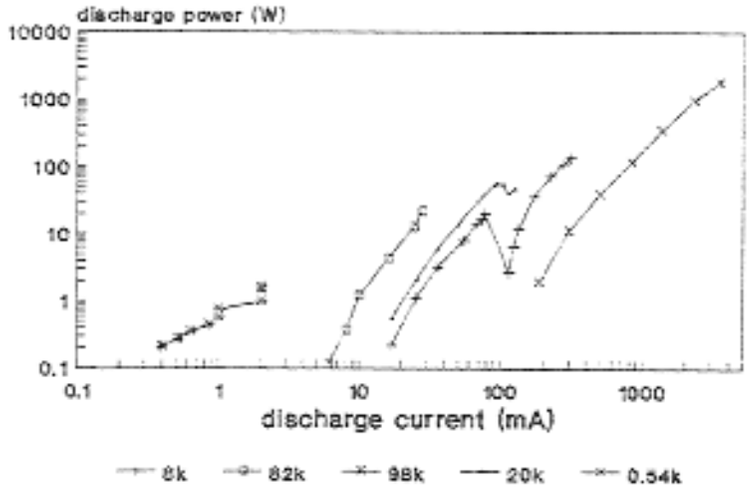

Fig 3.24 Power characterisics of some capacitive discharges

Priede found that $R_d \propto I_d^{-n}$, and substitution for R_d in the above equation gave

$$H_d' \propto I^{2-n} \qquad (3.29)$$

Equating the powers of I_d gave

$$a = 2-n. \qquad (3.30)$$

Priede found that n=1.36, which would give a=0.64. Thus the general form of the result $H_d' \propto I_d^a$ was consistent with Priede's results, but the value of the exponent found in these experiments was greater by a factor of 2–6 than Priede's results.

The discharge power–current characteristic was determined by the peak current and conditions in the initial stages of the discharge. Increasing the series resistance had the dual effects of increasing the discharge duration and determining the peak discharge current, which had a value close to V_B/R_r. The impulse at the wavefront due to discharge of electrode stray capacitances had a minor effect. The ratio $I_{dp}\ R_r/V_B$ was normally close to unity for discharge currents in the range 10^{-1}–10A. A value slightly less than V_B/R_r was normal as the discharge contributed a significant voltage drop. Discharges through powder in the current range $10^{-3}A<I_d<10^{0}A$ could be highly variable in voltage (fig 3.25). At low capacitance values the capacitor voltage could drop significantly from the breakdown value by the time the peak current was reached. At R_r=1Ω the discharge current was oscillatory and circuit inductive and capacitive impedances limited the peak discharge current to less than 5% of the V_B/R_r value.

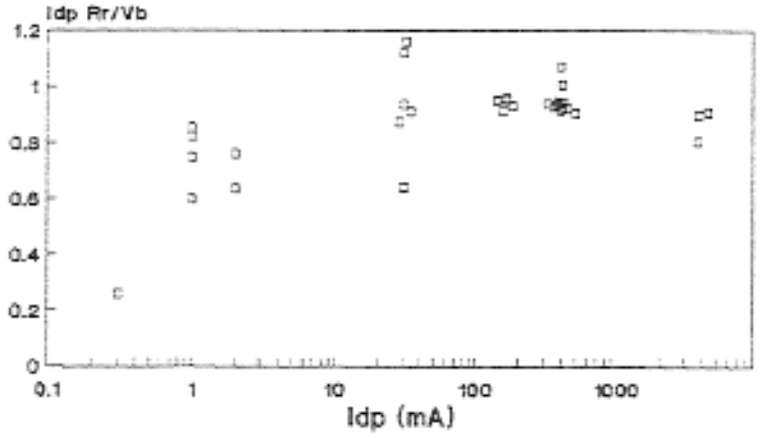

Fig 3.25 The ratio I_{dp} to V_B/R_s as a function of discharge current

The power dissipation at a given discharge current was a function of the peak current a discharge through air (fig 3.24) or pyrotechnic. The power dissipation in a discharge through pyrotechnic was more variable, particularly at discharge currents $<10^{-1}$A. The power dissipation H^{λ}_{dp} at peak current I_{dp} through air was nearly proportional to I_{dp}.

$$H^{\lambda}_{dp} = 470\ I_{dp}^{0.935} \qquad (3.31)$$

A thin unconfined powder layer could be much more easily ignited than the partially confined powder when high ($>8x10^5\Omega$) series resistance was used. When using partially confined powder, current pulses appeared before full breakdown occurred. This phenomenon was associated with a reduced rate of rise of voltage stored on the capacitor. The discharges prevented the recording of a full discharge waveform even if one occurred. The pulses were not observed when using the thin unconfined dust layer, and appeared to be linked to the immersion of the electrode tip in the dust layer. The pulse amplitudes were of the order 1mA, and durations of 25ns were typical. There was some variation in the pulse amplitudes but waveforms were very similar (fig 3.26), and around 60pC charge was transferred in the discharge. The phenomenon may be a form of corona discharge, with highly divergent fields produced in the presence of powder particles. It is not obvious why these discharges were not observed when lower series resistances were used, as corona inception should be independent of series resistance in the circuit. The explanation may be that in a higher resistance circuit the electrode voltage was significantly depleted by a corona pulse wheras at lower series resistance the electrode voltage was better maintained. A corona pulse at lower series resistance was therefore more likely to develop into full breakdown.

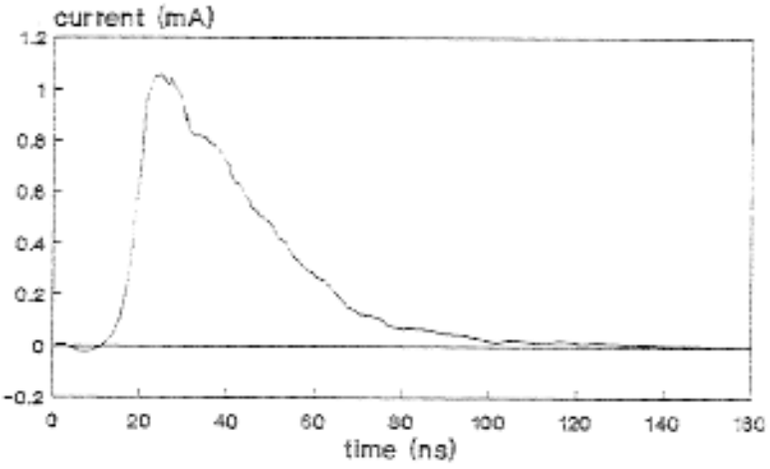

Fig 3.26 Trichel pulse like discharge

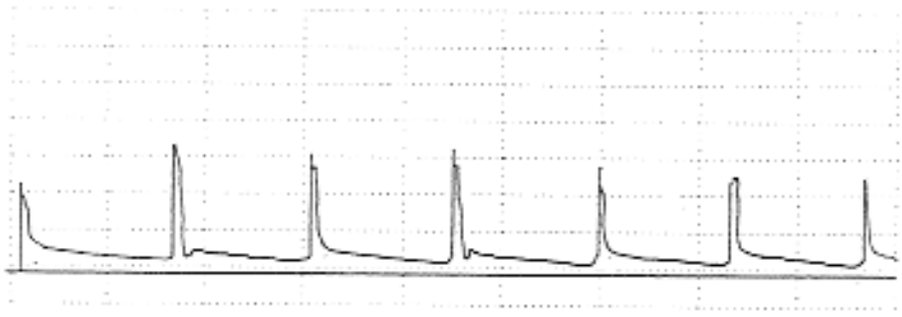

a) pulse train detail

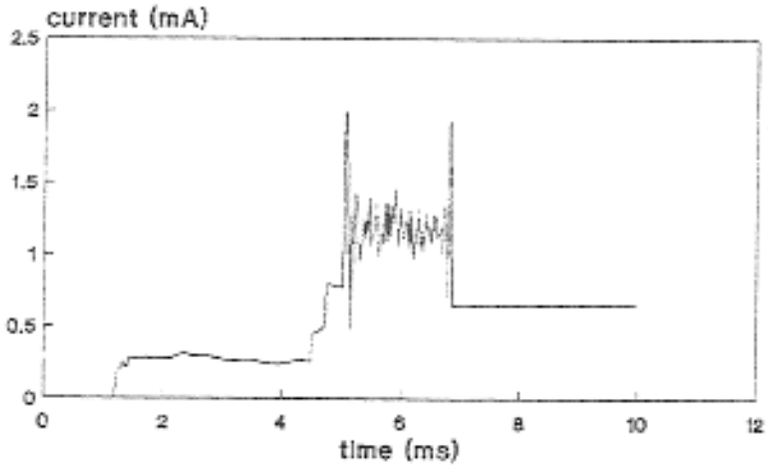

b) Pulse burst in discharge through pyrotechnic

Fig 3.27 Pulse train discharge

Pulse train discharges

At high values of circuit resistance ($>10^6\Omega$) the discharge often formed a train of fast pulses, with a low discharge current observed in between. A typical waveform (fig 3.27, Rs=2.77MΩ) showed 2ns pulses of 40mA amplitude at approximately 3MHz repetition rate. The charge transferred in each pulse was approximately 150pC. The pulses were clearly different from the pre-discharge pulses previously described, having faster risetimes, sharper peaks, and shorter durations with higher peak currents and transferred charge values. The pulses occurred during the waveforms rather than prior to breakdown. Different mechanisms were therefore implied. It is proposed here that non-linear behaviour of the discharge caused relaxation oscillations to be set up. Charge was stored on the electrode capacitance C_{lg} which discharged on breakdown. The 2.77MΩ resistance then limited the major circuit current to a value less than the sustain current of the discharge, and the discharge quenched. The electrode capacitance then charged up until the breakdown voltage was again exceeded. This breakdown could be achieved at a lower discharge voltage than the original breakdown of the gap as an ionised path could remain from the previous discharge. The 3MHz repetition rate is consistent with an electrode capacitance of the order 1pF.

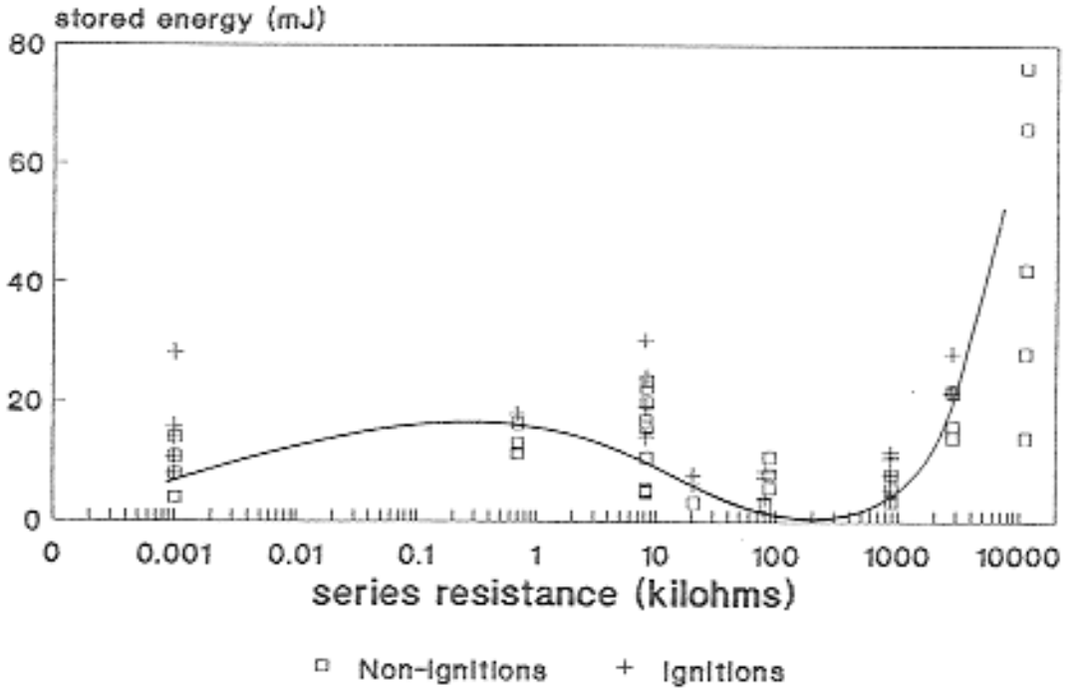

Fig 3.28 Stored energy for ignition as a function of series resistance

Ignition results

The ignition results were first displayed as a scattergraph of the stored energy against series resistance (fig 3.28) after Maki's example. All results (fixed electrode, approaching electrode, unconfined and partially confined) were included. Sensitivity reduced greatly above 10^6–$10^7\Omega$. Peak sensitivity appeared with circuit resistance in the 10^4–$10^6\Omega$ region. A region of lesser sensitivity a lower resistances gave way to increased sensitivity at circuit resistances of the order 1Ω. The characteristic therefore fitted the Type 2 sensitivity form. When stored energy was plotted against discharge current (fig 3.29) increased sensitivity could clearly be seen to be associated with the reduction of discharge current through the 10^0–10^{-1}A current (arc–glow transition) region. The characteristic showed strong evidence that ignition of the dust layer was improved for glow–like discharges over arc–like unidirectional discharges. No ignitions were obtained at less than 14mJ stored energy at discharge currents greater than 200mA. This corresponded to the region for which an arc–like portion formed a significant part of the waveform. The stored energy for ignition reduced considerably as the peak discharge current reduced through 0.2–0.1A. In the glow–like discharge region (<100mA) ignitions were obtained as low as 3.7mJ (at 50mA).

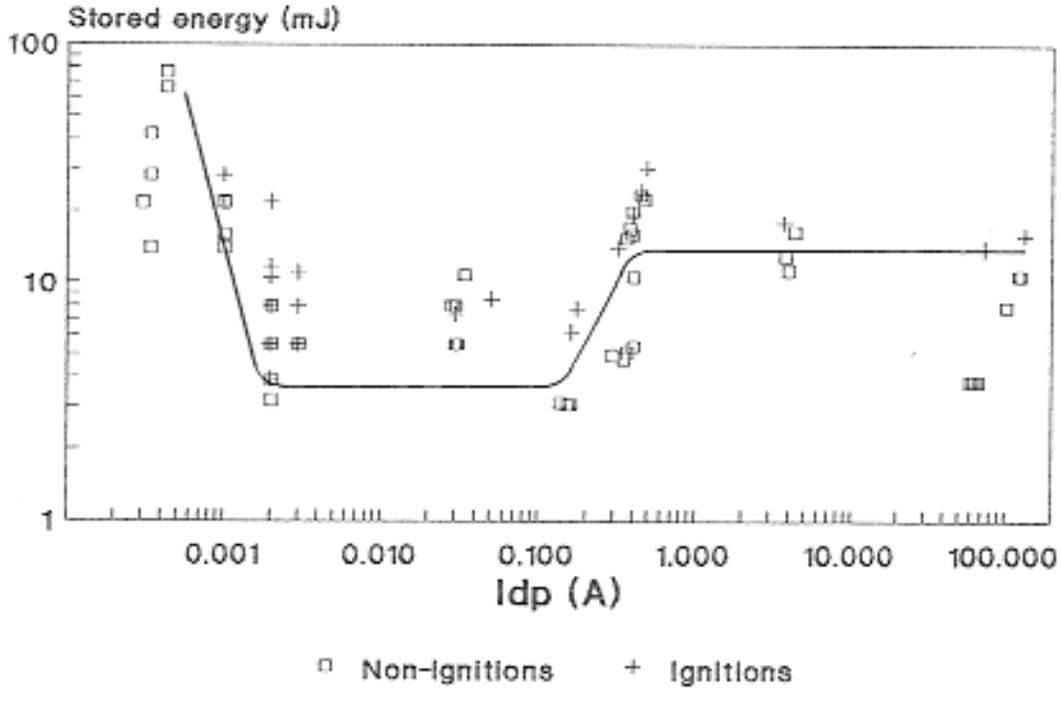

Fig 3.29 Stored energy for ignition as a function of peak discharge current

The ignition sensitivity reduced as the discharge current reduced below approximately 10^{-3}A. A change to the pulse train form of discharge could also occur in this current region. The truncation of the trailing part of the waveform could also occur at these low discharge current levels, consistent with the transition of the discharge from a conductive to a non-conductive state. The point of truncation was variable from discharge to discharge. It is likely that below a threshold current the energy input into the discharge became less than the energy losses and insufficient to maintain the conductive plasma channel. The lower limit of viable discharge current appeared to be in the 10^{-3}–10^{-4}A region.

Ignition results were also displayed as a function of the discharge duration in the form of the $R_f C$ product (fig 3.30). An optimum duration was indicated in the region R_f C = 0.2ms. Discharges at the minimum and to the right were found to be of glow-like or pulse train form. Discharges to the left of minimum were found to be transition or arc-like. Optimum duration occurred at the high discharge current end of the glow region. It is in this range that the glow discharge power is greatest. Reducing the discharge duration required an increase in discharge powert for the same energy, but this would lead to a switch to the less efficient arc-like discharge. Increasing the discharge duration implied a reduction in discharge power and a probable increase in heat losses from the discharge to the surroundings, leading to an decrease in ignition sensitivity.

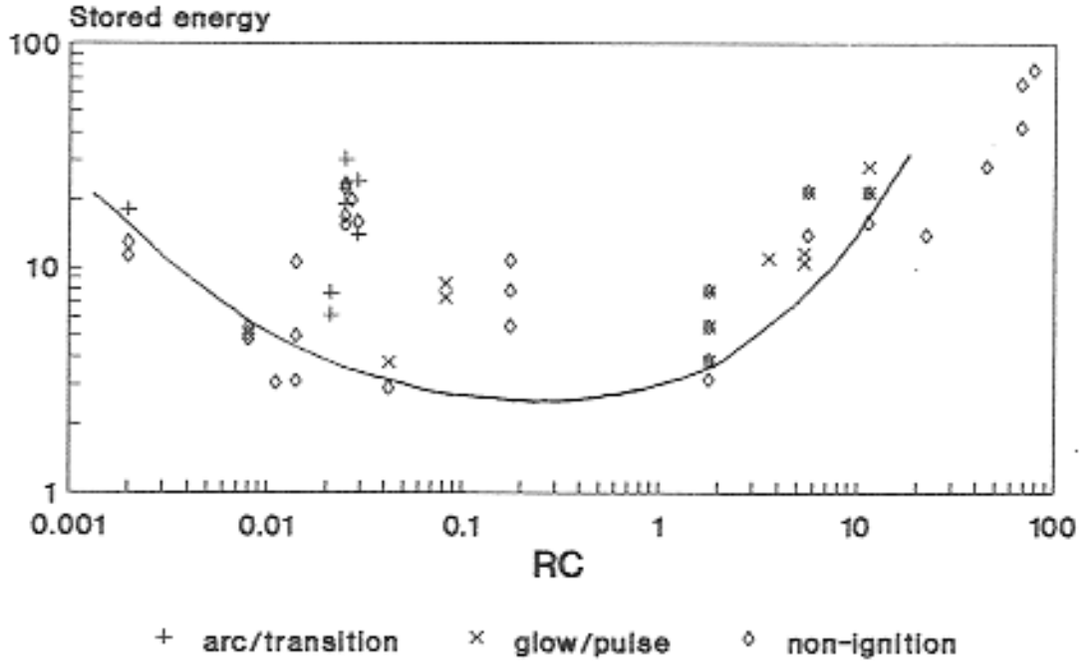

Fig 3.30 Ignition of pyrotechnic as a function of discharge duration in the form of R_f C product

An apparent increased sensitivity in terms of stored energy was associated with a change to glow-like discharge form. The glow discharge had a substantially greater cathode fall which led to increased power dissipation per unit current compared to the arc-like discharge. The glow like discharge was therefore more efficient at converting stored energy to a form available for the ignition process. The increase in discharge voltage drop from circa 50V to 400V or greater could account for account for a considerable increase in the proportion of stored energy dissipated in the glow-like discharge. Most of the increased voltage drop in a glow discharge occurs near the cathode, and this could perhaps account for polarity effects sometimes reported in the literature. Assuming all the capacitor voltage is presented accross the arc (V_a) or glow (V_g) discharge and circuit resistance R_r, the ratio of glow discharge power H_g' to arc discharge power H_a' is

$$\frac{H_g'}{H_a'} = \frac{V_g\ (V_c - V_g)}{V_a\ (V_c - V_a)}$$

This factor could account for a change in apparent sensitivity of a factor of 5-8 at V_c = 1kV for V_a = 50V and V_g = 400V. This is consistent with the observations here. In contrast, data in the literature often shows apparent sensitivity changes greater than this, and so other factors may play a part for other materials. A factor which may influence the sensitivity is the geometry of the discharge channel. The arc discharge in air is characterised by a narrow discharge channel with high current density, wheras the glow discharge has a broad discharge channel of variable diameter with a fairly constant current density. Whilst the dynamics of the arc-like and glow-like discharge channels through powder are unknown, it is possible that the glow-like discharge heats a greater volume of material with a broader discharge channel, which may favour ignition.

Unfortunately a significant proportion of the trials did not yield successful discharge energy calculation results. In practice only unidirectional discharge energies were successfully calculated. The author is unaware of a theoretical reason why the energy calculation of oscillatory discharges should fail, and the matter remains unresolved. At the lowest values of circuit resistance (1Ω, consisting of the current sense element alone) high values of discharge current ($>10^2$A) caused failure of the data transfer and prevented calculation of the discharge energy. This was probably due to ground loop difficulties. When high series resistances were used a pulse-train waveform was produced. The RLC circuit model used in the calculations was inadequate and the energy calculation invalid for these waveforms.

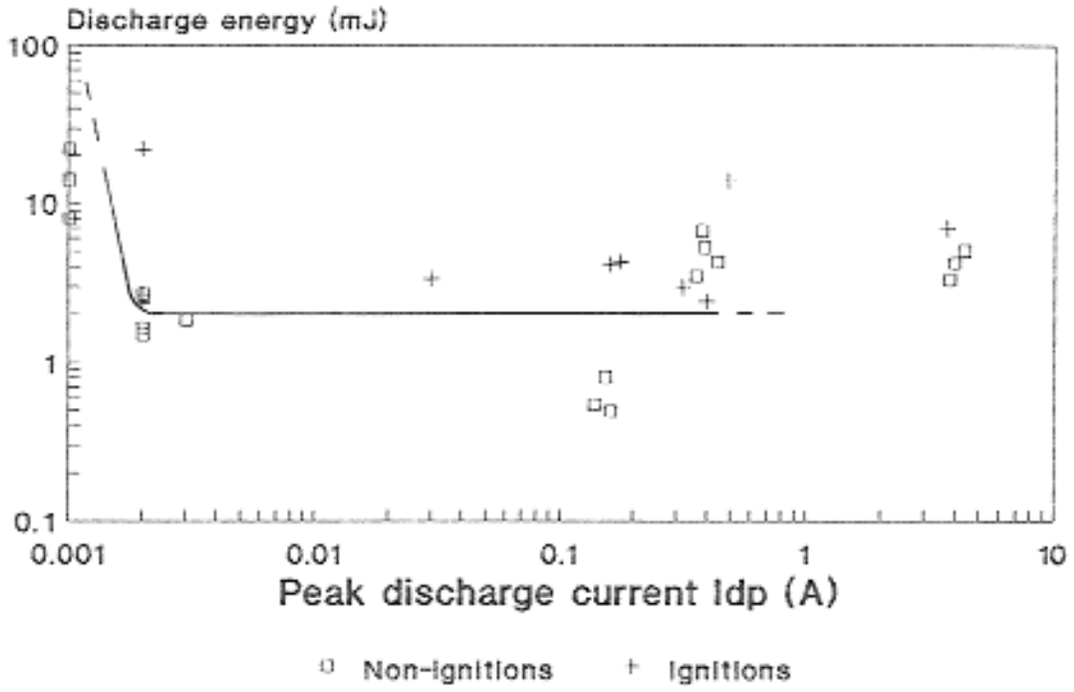

Fig 3.31 Discharge energy for ignition as a function of peak discharge current

Discharge energy results that were obtained appeared to show a relatively constant discharge energy for ignition over the range 10^{-3}–10^{0}A (fig 3.30). There was insufficient data to conclusively show the form of the sensitivity curve in the $<10^{-3}$A and 10^{-1}–10^{0}A current regions those regions. However, it seems reasonable that the reduction of sensitivity in terms of stored energy observed at low discharge currents is probably reflected in a similar behaviour with respect to discharge energy. The behaviour in the 10^{0}A current region requires further elucidation.

3.4 PULSE DISCHARGE MEASUREMENTS

3.4.1 120ns NR pulse discharges in gas mixtures

The pulse breakdown voltage of air and hydrogen-air mixture by a 120ns NR pulse was greatly reduced by the injection of ions from a corona discharge (fig 3.32). This reduced the energy stored in the gap capacitance at breakdown. A discharge gap of 0.7mm in air, having capacitance 0.5pF could require 12kV pulse to break down the gap without corona, and the stored gap energy would be 36μJ. A similar gap, seeded with ions using corona, could break down under 3kV, with a stored energy of only 2.2μJ. The pulse breakdown voltage increased proportionally to gap as predicted by Paschen's law, as the working pd range was restricted and to the right of the Paschen minimum. Breakdown potential was reduced when 30% hydrogen was present in the gas mixture (fig 3.32). The measured breakdown values for air yielded the relations

$$V_B \alpha\ 3520\ d + 1220 \qquad \text{(V) (with corona)} \qquad (3.32)$$

$$V_B \alpha\ 16100\ d + 760 \qquad \text{(V) (no corona)} \qquad (3.33)$$

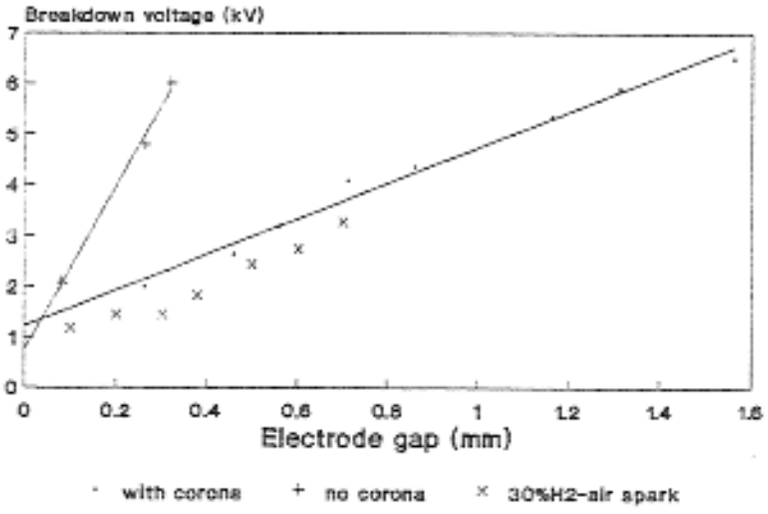

Fig 3.32 120ns pulse breakdown of air as a function of the electrode spacing

Pulse breakdown characteristics were dependent on the pulse overvoltage and the conditions and material within the electrode gap. A typical 120ns pulse discharge waveform appeared to have 3 distinct stages. (fig 3.33). In the first (pre-breakdown) stage, a small pulse of current could be seen. This was due to displacement current in the gap capacitance, and could be seen to be following the rate of change of the driving pulse rising edge. The displacement current caused a small increment of energy to be calculated, equal to the energy stored in the C_{12} electrode capacitance.

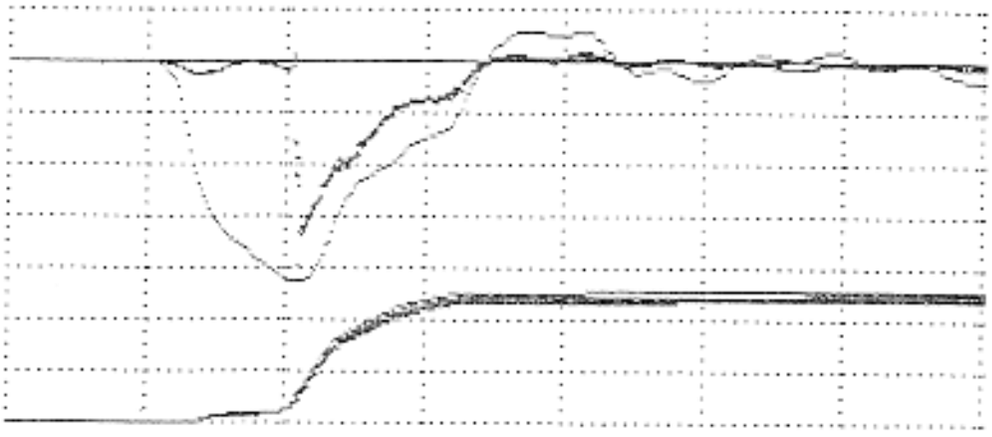

a) V_p=3270

vertical 99mA/div horizontal 100ns/div

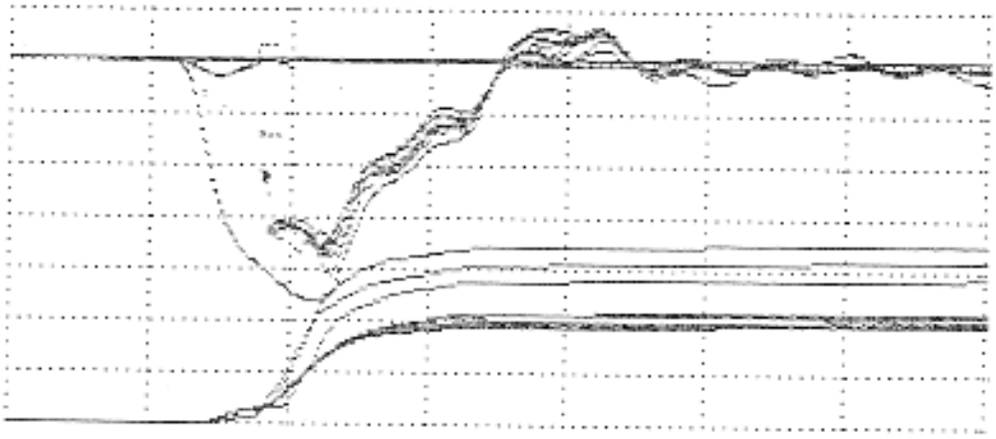

b) V_p=3570

vertical 99mA/div horizontal 100ns/div

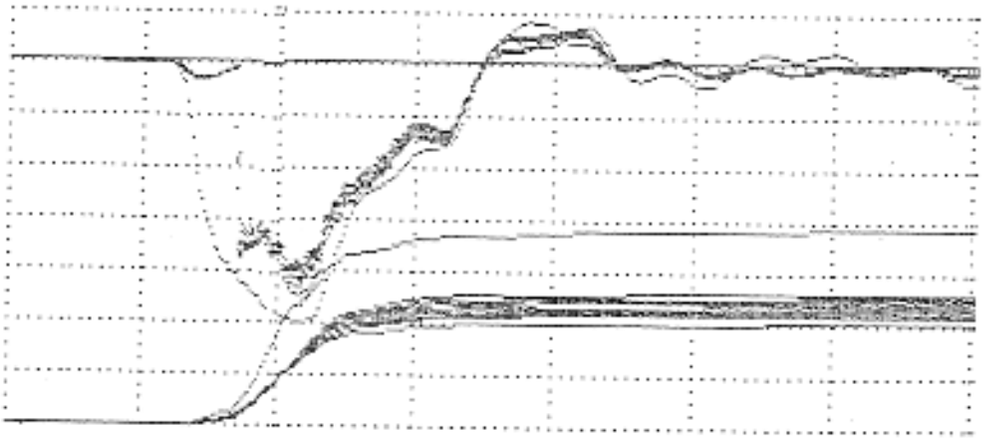

c) V_p=3860

vertical 99mA/div horizontal 100ns/div

Fig 3.33 Variation in breakdown delay with pulse voltage

A delay between the rise of pulse voltage and discharge gap breakdown was most pronounced when low overvoltages were used. This caused variation in discharge duration and discharge energy, and was particularly significant for short discharges of 100ns duration or so, where the variation was of similar magnitude to the pulse duration. The effect of overvoltage in enhancing the speed of breakdown can be seen by comparison of the waveforms in fig 3.33. Pulse voltages of 3860, 3570 and 3270V gave breakdown delays of 28ns, 39ns and 74ns respectively. In the last case the pulse voltage only slightly exceeded the breakdown value.

The second and third stages of the discharge occured after breakdown, which was clearly seen as a very fast step rise in the current waveform. The second stage had a higher rate of energy rise, and commonly lasted about 40ns after breakdown. In the third stage the rate of energy rise settled to a lower value dependent on the discharge current.

The discharge characteristics were classified similarly to capacitive discharges, as a function of discharge current (fig 3.34). The discharge current waveform in general followed the applied pulse voltage waveform, except at low currents when a pulse train could spontaneously form. Applied pulse waveforms were unidirectional and so discharge current waveforms were in general similar. Arc, glow and pulse train discharges were observed.

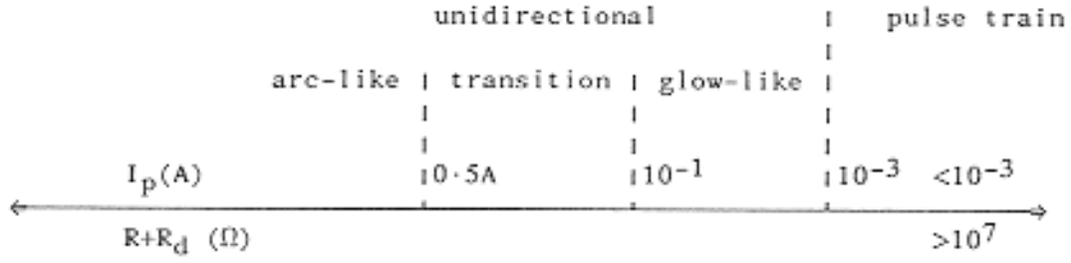

Fig 3.34 Pulse discharge waveform types as a function of discharge current

3.4.2 120ns pulse discharge energy as a function of discharge current

This investigation of a restricted range of inter-electrode gap, series resistance and pulse voltage found results which could be described by simple relationships. These relationships have been explained in terms of the discharge as a current driven phenomenon, ie. the discharge resistance was considered to be largely a function of discharge current for a given electrode geometry and materials. A relation between discharge energy, discharge current I_d, the inter-electrode gap d, the discharge duration and empirically determined constants was sought.

Priede reported that $R_d\ I_d^n$ = constant was valid for aperiodic and periodic waveforms in a CD circuit. This equation was rearranged, with a constant of proportionality K_d, as

$$R_d = K_d\ I_d^{-n} \tag{3.34}$$

The power dissipated in the discharge was then

$$H_d' = I_d^2\ R_d = K_d\ I_d^{2-n} = K_d\ I_d^{-a} \tag{3.35}$$

Here $a = -(2-n)$. The discharge energy was the integral of H_d' over the duration of the discharge θ. For a rectangular waveform, the integral would be

$$H_d = H_d'\ \theta = \theta\ K_d\ I_d^{-a} \tag{3.36}$$

hence for constant duration θ,

$$H_d \propto I_d^{-a} \tag{3.37}$$

I_d was largely determined by the series resistance R_r and the pulse voltage V_p, but the circuit resistance $R_r \approx R_s$. Thus

$$I_d = V_p/R_s \tag{3.38}$$

Substituting this in the energy equation yielded

$$H_d \propto (V_p/R_s)^{-a} \tag{3.39}$$

$$H_d \propto V_p^{-a}\ R_s^a \tag{3.40}$$

Discharge energy H_d and series resistance R_s data for a range of conditions (fig 3.35) yielded a straight line graph when plotted on logarithmic scales. This implied a power relationship between the discharge energy and circuit resistance.

$$\log(H_d) = a\ \log(R_s) + b \qquad (\mu J) \tag{3.41}$$

$$H_d = 10^b\ R_s^a \qquad (d \text{ and } V_p \text{ constant}) \tag{3.42}$$

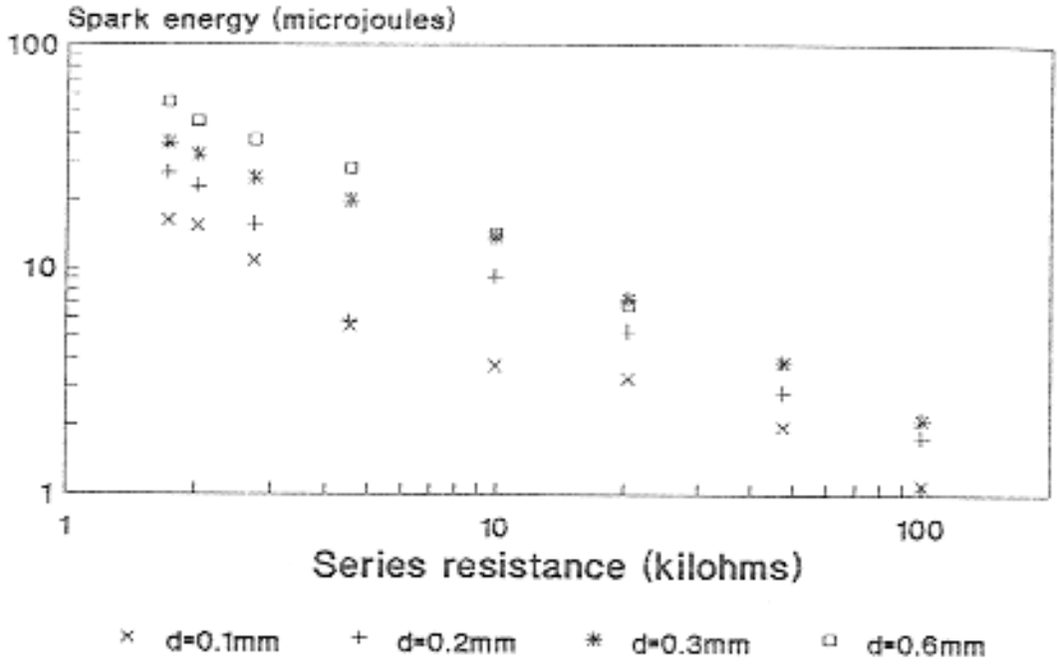

Fig 3.35 120ns pulse discharge energy as a function of series resistance

The parameters a,b varied approximately linearly with electrode gap over the limited range of electrode spacing 0.1mm < d < 0.5mm, corresponding to

$$a = -0.389\ d - 0.5676 \qquad (3.43)$$

$$b = 2.509\ d + 2.870 \qquad (3.44)$$

Priede's value of $a = (2-n) = 0.64$ lay within the range of these results. An equation for the discharge energy as a function of V_p was similarly predicted.

$$H_d \propto V_p^{-a} \qquad (3.45)$$

By suitable choice of a constant of proportionality, the data could be seen to resemble $H_d \propto V_p^{0.64}$. This is illustrated in fig 3.36, where the experimental data was plotted against the curve $H_d = 165\times10^{-9}\ V_p^{0.64}$ (Joules). The curve could appear linear for limited range of V_p.

The success of this analysis led to the conclusion that the relation $R_d\ I_d^n$ = constant was applicable in the 120ns gas discharge experiments, although the constants vary with electrode geometry. This equation was used to derive a predictive equation for discharge energy, so far as was possible. Equation (3.36) stated, for a rectangular pulse;

$$H_d = K_d\ \theta\ I_d^{-a} \qquad (3.36)$$

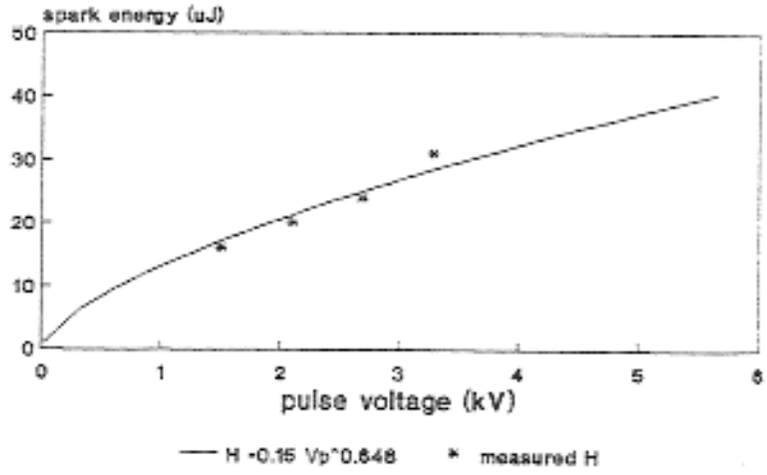

Fig 3.36 Theoretical and experimental discharge energy as a function of pulse voltage

Comparing equation (3.36) with equation 3.42 gave

$$H_d = K_{d1}\ 10^b\ d\ \theta\ I_d^{-a} \qquad (3.46)$$

When generalised for a non-rectangular waveform, this became

$$H_d = K_{d1}\ 10^b\ d \int_0^T I_d^{-a}\ dt \qquad (3.47)$$

Ideally, this integral should be compared with a number of waveform sample and energy results, to evaluate K_{d1} and to check that the results conform correctly. In practice, the effort involved in achieving this was large, and the level of correlation was not expected to be high, so the simpler equation for rectangular waveforms was used as an approximation. The constants K_{d1} a and b probably change with different electrode configurations and gases, and n has been observed to be slightly dependent on d. The discharge energy for a given series resistance and pulse voltage linearly increased with gap width. The results conformed reasonably well to

$$H_d \propto d \qquad (V_p,\ R_s \text{ constant}) \qquad (3.48)$$

$$H_d = 79.4\ d + 13\ (\mu J) \qquad (R_s = 1712\Omega \text{ and } V_p = \text{constant})$$

3.4.3 120ns NR pulse ignition of 30%H2–air mixture

The ignition results are presented as energy–duration scattergraphs for d=0.5mm (fig 3.36), 0.6mm and 0.7mm. The duration of the discharge was significantly variable even though a constant reference pulse duration was used. The greatest factor in this was the breakdown delay due to formative lag, especially at low overvoltages. At high R_s resistance values the charging time R_s $(C_{1g}+C_{12})$ was significant.

The lowest ignition occurred at 22μJ with d=0.6mm. As energy was increased from a low value the ignition probability rose from zero through a transition band to 100%. The transition band was 5–10μJ in range. The values given should not be regarded as a minimum ignition energy. A much larger number of results would be required to give a statistically representative database and no attempt was made to find the optimum over a wide range of conditions.

Table 3.4 Ignition of 30% H2–air mixture using 120ns pulse discharge.

gap	LIE	0%IE	100%IE
0.5	43	42	45
0.6	22	21	31
0.7	25	23	29

LIE –Lowest measured ignition energy under given conditions.
0%IE –Highest energy at which no ignitions occurred.
100%IE –Lowest energy at which 100% ignitions occurred.

3.4.4.1 FRED pulse discharge studies

The FRED reference pulse waveform was very similar in some respects to many capacitance discharges. The applied pulse waveform had a fast rise and exponential decay, which often gave rise to a similar current waveform. In contrast to the CD case, the FRED reference pulse waveform could be maintained while the discharge current, and hence power and energy, were changed by adjustment of the discharge circuit resistance. FRED pulse discharges through air and SR10 pyrotechnic powder layer were studied. The breakdown voltage in the case of a pyrotechnic powder filled gap was variable but did not prove to be much greater than an air filled gap. This was probably because the FRED pulses used were sufficiently long in duration for the breakdown delays to be insignificant compared to the waveform duration. A high

overvoltage was therefore not required for fast breakdown, and no artificial seeding of the gap with ions was required. It is possible that the presence of dielectric powder was sufficient to create a non-uniform electric field which could enhance breakdown.

3.4.4.2 The heat pulse duration

When initially investigating the pulse ignition phenomena the duration of the discharge event was defined as the current discharge half peak amplitude duration θ. Some discharges, in particular glow-like discharges through pyrotechnic powder, did not preserve the pulse waveform. It was felt that the θ definition was only useful in comparing similar waveforms. Inspection of equation 3.47 showed that waveform and amplitude were both important in the convertion of discharge current to heat energy, and this equation did not take into account the additional differences between arc-like and glow-like discharge forms. (This equation was derived from data from short duration discharges and is not necessarily applicable to long duration FRED pulse discharges). In addition, the software algorithm used to calculated θ duration did not sucessfully cope with double peak or other uncoventional waveforms.

An additional definition of duration θ_h based on the heat pulse was adopted for investigation. A similar approach has been used by Eckhoff (1975). The heat pulse duration θ_h was defined as the time taken to dissipate the 90% of the energy which fell between 5% and 95% of the final discharge energy value. Consideration of heat pulse characteristics in relation to the ignition process is highly consistent with the energy oriented philosophy of ignition experiments. In addition, the θ_h duration was easily calculated automatically from the energy results (or graphically measured in retrospect from an energy curve) and was insensitive to waveform differences. The measured values of θ and θ_h were approximately related, but considerable variations could occur (fig 3.37). Consistent values for both were obtained in the arc-like discharge region ($I_d > 10^{-1}A$) although for a constant pulse waveform, θ was also constant but θ_h increased slightly with increasing discharge current. This was due to the effect of truncation of the discharge waveform at low discharge current in the waveform tail. In the glow discharge region ($I_d < 10^{-1}A$) the relationship between θ and θ_h was most variable.

In order to investigate the discharge as a heat pulse and confirm discharge characteristics, waveform data was imported into Lotus 123 and the discharge power, voltage, and resistance was calculated.

3.4.4.3 Arc and glow-like pulse discharges through pyrotechnic powder

FRED pulse discharges in air and powder had arc-like and glow-like characteristics similar to those found in capacitance discharges. The current waveform largely followed the reference pulse. The difference between the discharge current and their reference often appeared nearly constant during the arc-like and glow-like phases due to the near constant discharge voltage. Discharge energy increased more rapidly during the glow-like part of the waveform. As the current fell to a low value the discharge could truncate (fig 3.42b).

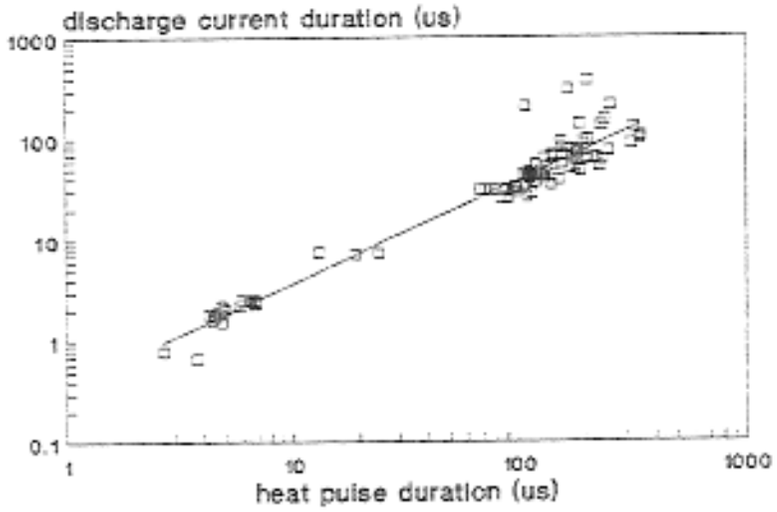

Fig 3.37 The relationship between heat pulse duration and discharge duration

Arc-like discharges

At higher currents (>0.5A) the reference and discharge currents of arc like discharges through air or through powder could be almost indistinguishable, as in the igniting discharge of fig 3.38. This was due to the low discharge voltage (of order 50V) of the arc-like waveform. If much of the discharge was in the arc state, as at higher discharge currents, the discharge current was close to the reference value for much of the waveform, a low MRF was produced. The discharge of fig 3.38 had an MRF of 0.2 and was almost entirely arc-like. The low value of MRF signified that digitisation resolution could be a limiting factor in the accuracy of the calculations.

The arc-like discharge appeared little affected by the presence of powder. This may be due the small diameter of an arc, allowing it to establish a path through the interstices between the particles. The shock wave associated with the arc could also displace powder material from the channel. Where the discharge commenced with an arc-like phase, the arc channel could establish a discharge path through the powder layer. A subsequent normal glow-like discharge could perhaps then follow the prepared channel with relative ease.

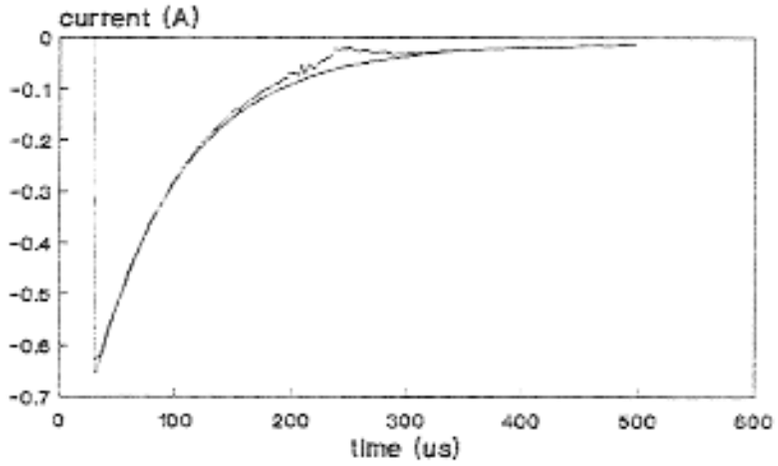

a) Reference and discharge currents

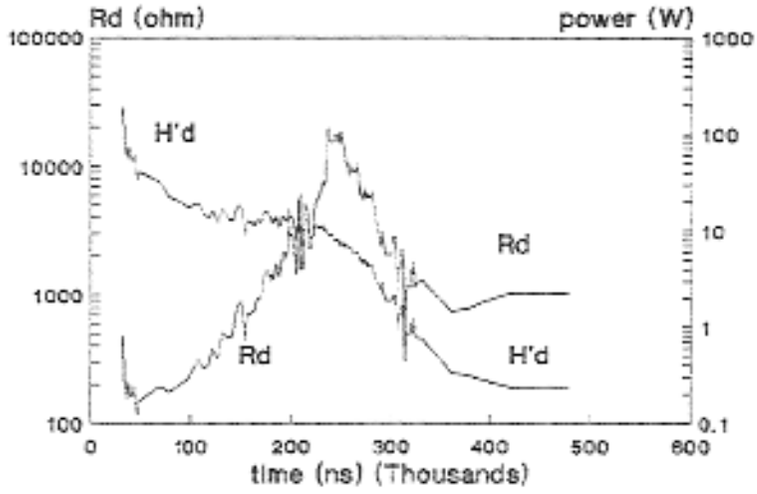

b) Discharge effective resistance and power

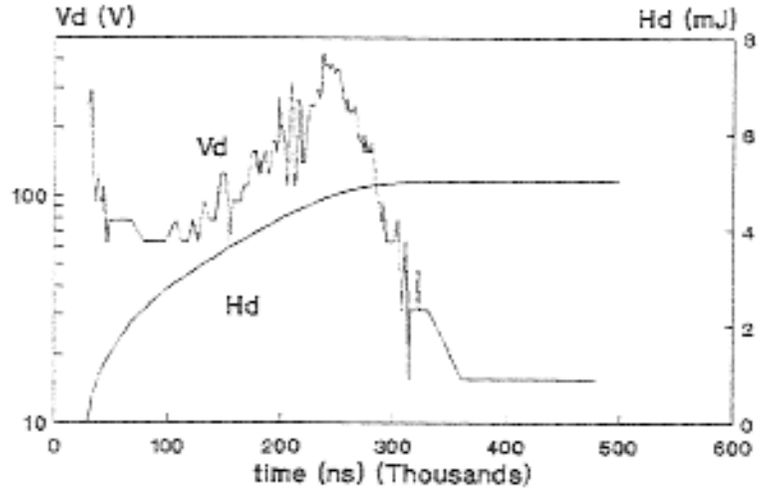

c) Discharge voltage and energy

Fig 3.38 Arc-like discharge current, voltage, power energy and resistance

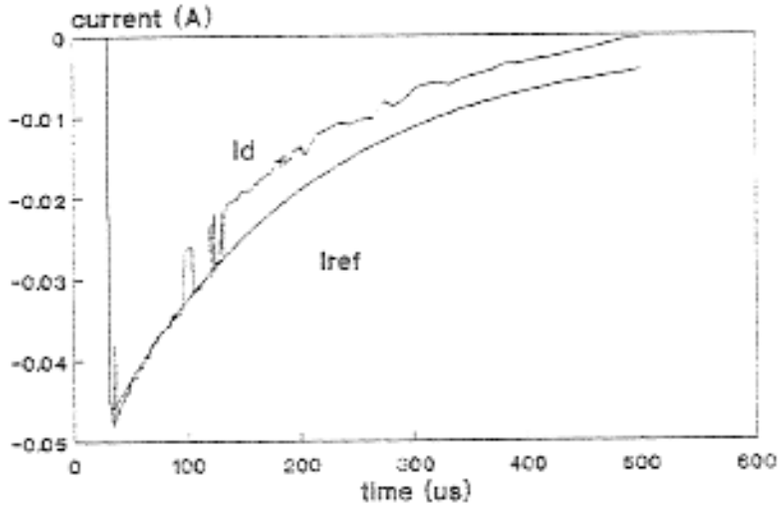

a) Reference and discharge currents

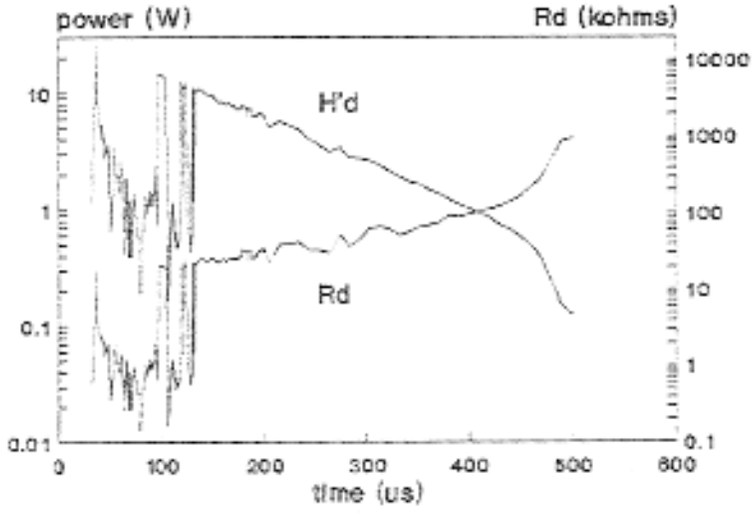

b) Discharge effective resistance and power

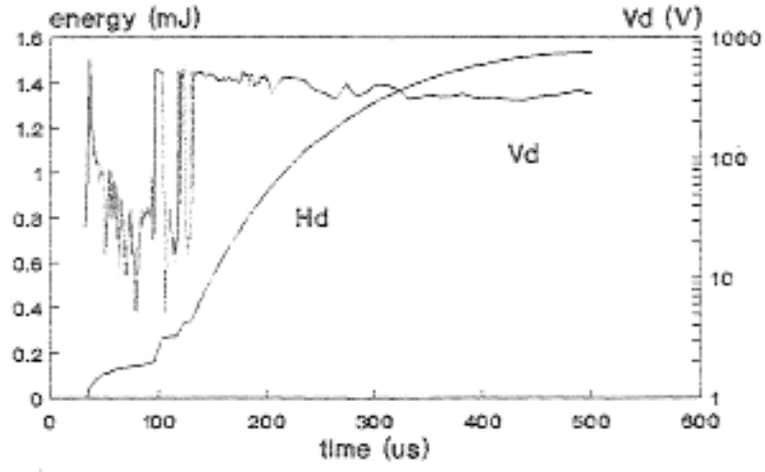

c) Discharge voltage and energy

Fig 3.39 Arc-glow transition discharge current, voltage, power energy and resistance

Arc-glow transitional discharges

If an arc-like stage was present the discharge current in this part was similar to arc-like waveform characteristics described above. Discharge voltage was of the order 50V in this region (fig 3.39). Transition to glow-like discharge was accompanied by a rise in discharge voltage to around 400V, although considerable fluctuation was observed. The discharge power increased by about an order of magnitude on transition to glow-like discharge. Truncation of a discharge was characterised by an abrupt increase in the calculated discharge resistance and the fall of discharge current to a low value. The MRF of low and intermediate current discharges (< about 0.5A), which had substantial parts of the waveform in the glow state, was generally in the range 1-10. Similar characteristics could be observed in arc-glow discharges through air and pyrotechnic layer.

Marked differences often were noted in the characteristics of the final stages of the discharge, however. An air discharge was almost always terminated by visible truncation (fig 3.41a) with the discharge current falling to near zero. In contrast, the current in a discharge through pyrotechnic often approached the reference value by one of two ways. One form feature a gradual approaching of the discharge current to the reference value (fig 3.41b). A second form featured an an abrupt decrease in discharge current (often to near zero) followed by a gradual increase in discharge current to the reference value (fig 3.38, 40). The discharge voltage and resistance abruptly increased simultaneously with the decrease of current, but reduced gradually to a low value less than expected for arc or glow discharge regimes. The step reduction in current may be due to disruption of the discharge by local ignition. The behaviour was also observed, however, in waveforms where propagating ignition did not take place.

In order to explain this it is postulated that some of the powder material formed a conductive bridge between the electrodes. Conductive reaction products or molten material could bridge the electrode space. This could effectively short circuit the electrodes, reducing the "discharge voltage" and energy input to a low level. A consequence of this was that the heat pulse duration in affected discharges could be shorter than expected from the current waveform duration. This was particularly marked in low current discharges where an arc-like phase was not present (fig 3.43.45a, 48). Further increase in the applied pulse duration tended to have little effect on the heat pulse duration. This factor underlined the necessity to use a heat pulse based discharge duration rather than a current waveform based definition.

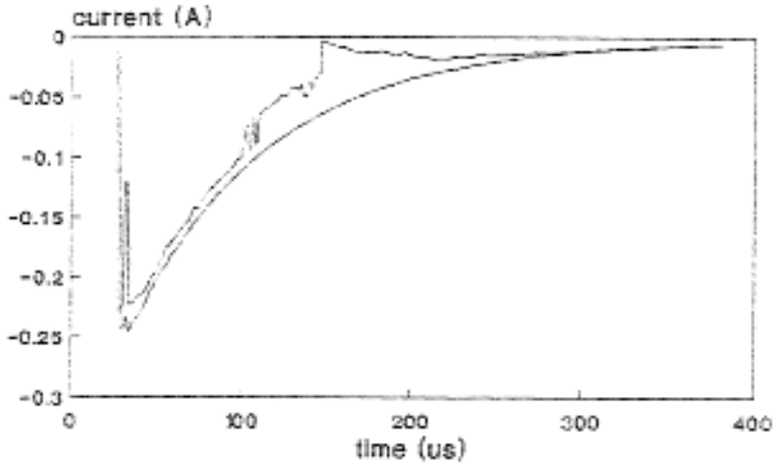

a) Reference and discharge currents

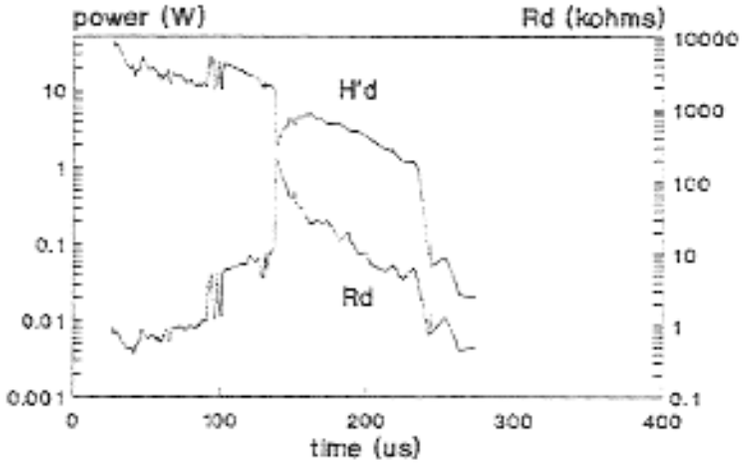

b) Discharge effective resistance and power

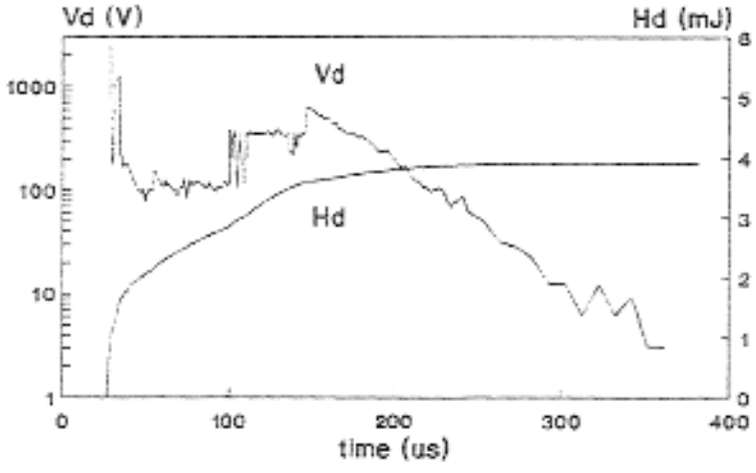

c) Discharge voltage and energy

Fig 3.40 Arc-glow transition discharge current, voltage, power energy and resistance

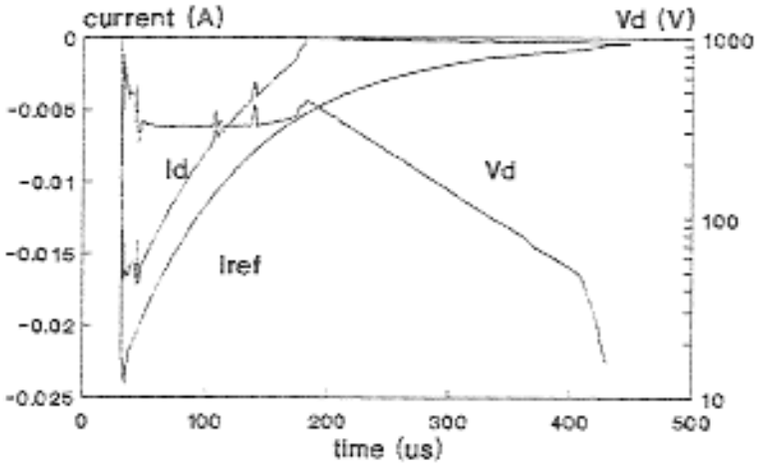

a) Discharge in air

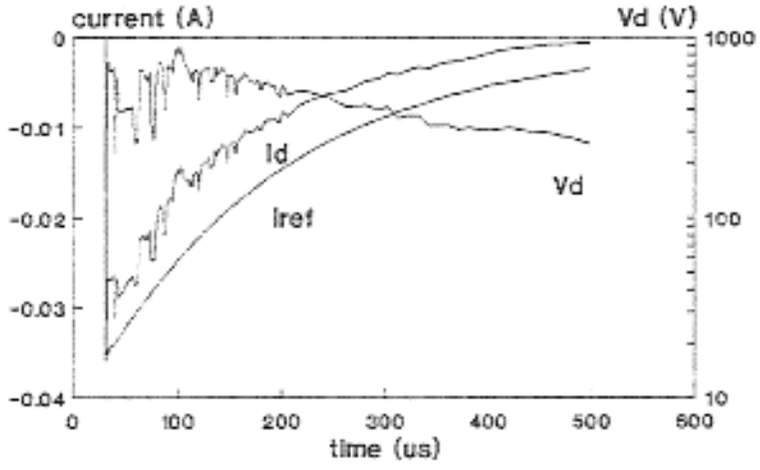

b) Discharge in pyrotechnic

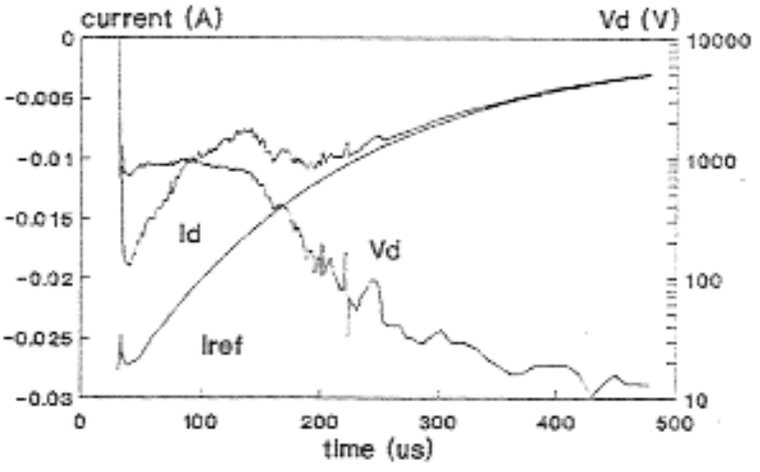

c) Discharge in pyrotechnic

Fig 3.41 Glow-like discharge waveforms

Glow-like discharges

The low current discharge through pyrotechnic dust in which the arc-like phase was absent was rather varied (fig 3.41). A typical discharge had a peak current substantially lower than the reference pulse. The initial stages often featured very high discharge voltages (500-1000V) for substantial periods of time and often did not follow the reference waveform. This may signify a modified (abnormal) glow regime.

Glow discharges are far larger in diameter than an arc and require a large cathode area. Cathode area could be restricted by contact with the powder, and if the reduced contact area were insufficient then an abnormal glow cathode could be the result. In addition, the discharge must percolate through a large volume of powder material of high thermal conductivity. Normal cathode secondary ionisation processes are probably inhibited by the presence of powder filling the electrode space. These factors could account for the high discharge voltages observed in the low current discharge waveforms.

3.4.4.4 FRED pulse ignition of SR10 pyrotechnic

Display of the FRED pulse ignition of pyrotechnic as a function of series resistance had little meaning in the context of pulse discharge ignition. Series resistance did not affect the waveform duration, and the power of the discharge was a function of the discharge current, determined by series resistance and pulse voltage together. The ignition scattergraph was therefore plotted as a function of discharge current (fig 3.43). A U-shaped sensitivity profile was apparent with a maximum sensitivity close to I_{dp}=100mA. Sensitivity appeared to decrease significantly as I_{dp} decreased towards 10mA or increased towards 1A. The range of discharge durations was rather narrow and no characteristic curves with respect to θ or θ_h could be determined.

In the spirit of seeking heat pulse parameters the an ignition scattergraph as a function of I_{dp} and a discharge power parameter H_d/θ_h was examined (fig 3.45). This implied a minimum of 0.8W at a discharge current of 100mA. This curve, however, was unsatisfactory in its lack of data below the implied curve except in the 10^{-2}-10^{-1}A current region.

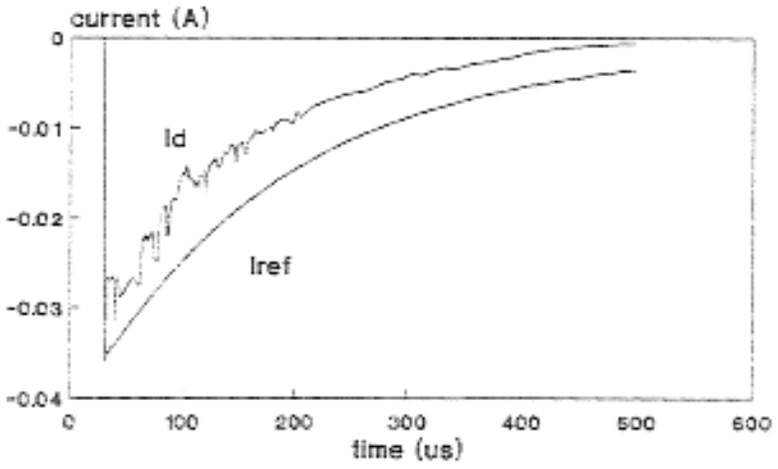

a) Reference and discharge current

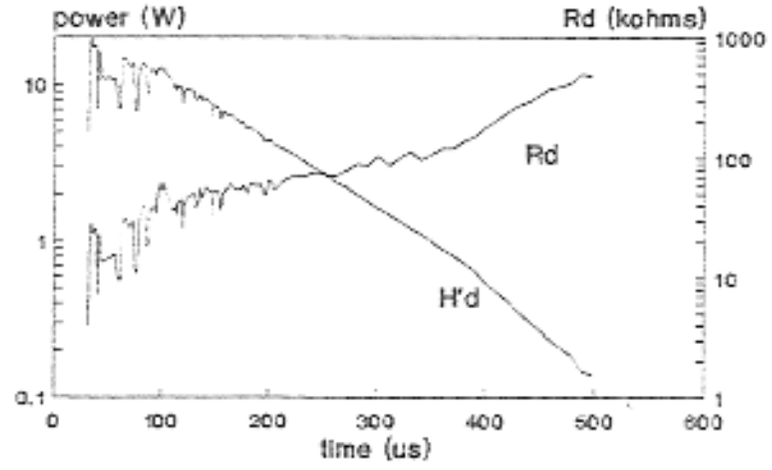

b) Discharge effective resistance and power

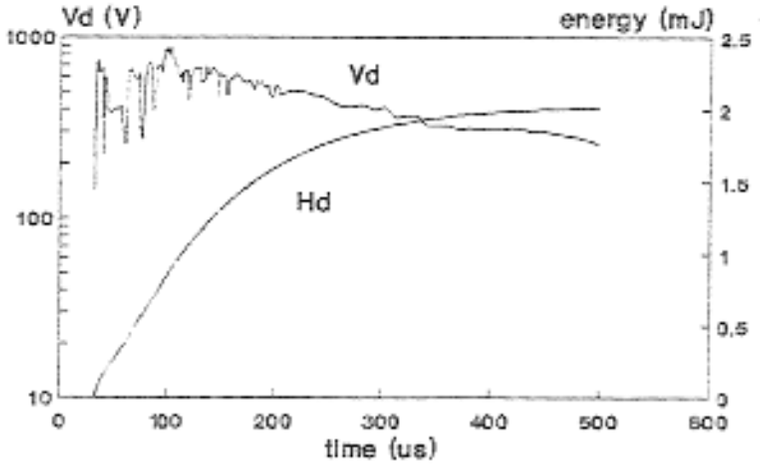

c) Discharge voltage and energy

Fig 3.42 Glow-like discharge current, voltage, power energy and resistance

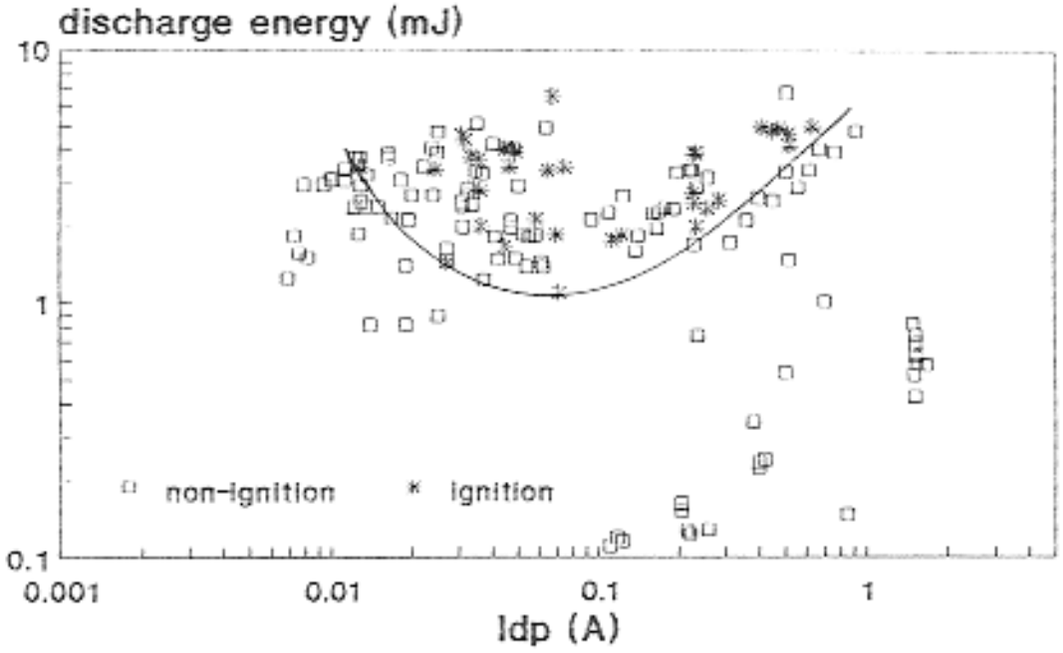

Fig 3.43 Pulse ignition energy of pyrotechnic as a function of peak discharge current

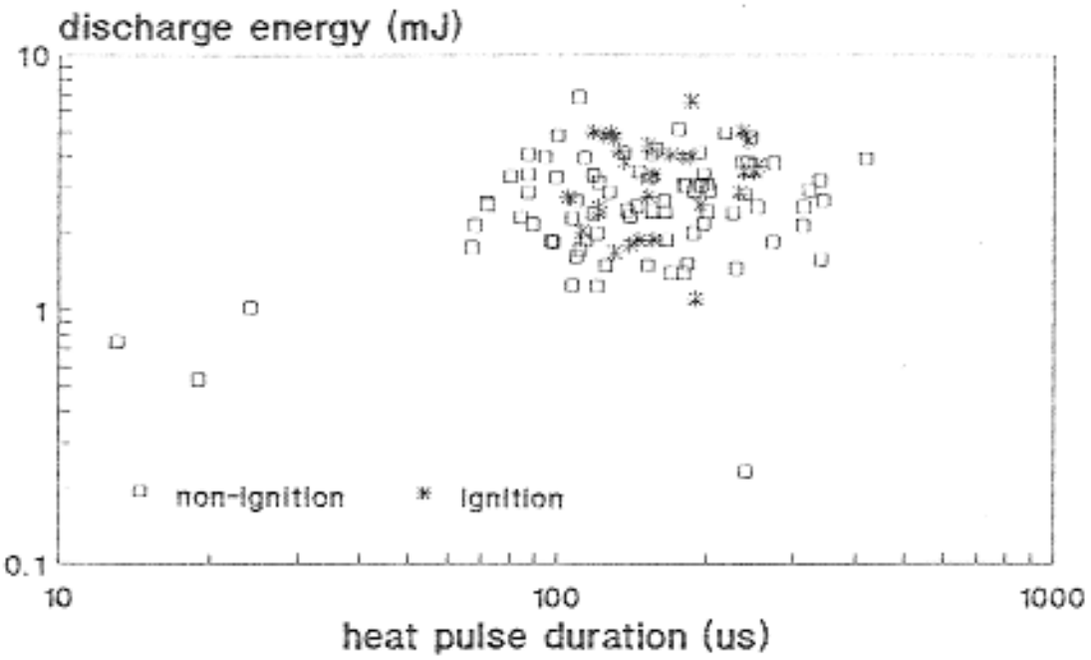

Fig 3.44 Pulse discharge ignition energy of pyrotechnic as a function of heat pulse duration

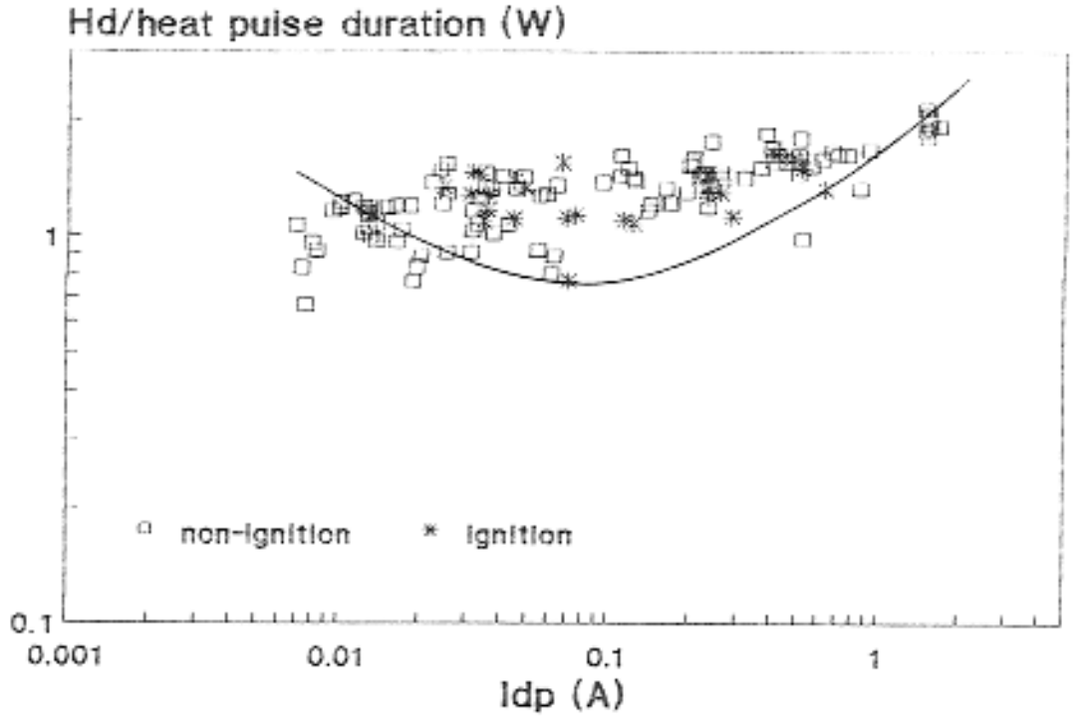

Fig 3.45 The ratio of pulse discharge ignition energy to heat pulse duration as a function of peak discharge current

It was clear in all these illustrations that the energy range from 0%–100% ignitions was wide. This can be explained as due to variable powder combustion properties as a function of the poorly defined powder pile. The variability of compaction, particularly when combined with variable confinement, must affect the heat transfer properties of the material as well as the proximity of the solid reagents. It is suggested that the problem of definition of dust sample compaction and confinement conditions is probably the most serious difficulty to be solved in the standardisation of this type of ignition test.